Neuroimaging of Spinal Cord and Cauda Equina Disorders

By Felix E. Diehn, MD; Karl N. Krecke, MD, FACR

REVIEW ARTICLE

CONTINUUM AUDIO INTERVIEW AVAILABLE ONLINE

ABSTRACT

PURPOSE OF REVIEW: **This article reviews the neuroimaging of disorders of the spinal cord and cauda equina, with a focus on MRI. An anatomic approach is used; diseases of the extradural, intradural-extramedullary, and intramedullary (parenchymal) compartments are considered, and both neoplastic and non-neoplastic conditions are covered. Differentiating imaging features are highlighted.**

RECENT FINDINGS: **Although T2-hyperintense signal abnormality of the spinal cord can have myriad etiologies, neuroimaging can provide specific diagnoses or considerably narrow the differential diagnosis in many cases. Intradural-extramedullary lesions compressing the spinal cord have a limited differential diagnosis and are usually benign; meningiomas and schwannomas are most common. Extradural lesions can often be specifically diagnosed. Disk herniations are the most commonly encountered mass of the epidural space. Cervical spondylotic myelopathy can cause a characteristic pattern of enhancement, which may be mistaken for an intrinsic myelopathy. A do-not-miss diagnosis of the extradural compartment is idiopathic spinal cord herniation, the appearance of which can overlap with arachnoid cysts and webs. Regarding intrinsic causes of myelopathy, the lesions of multiple sclerosis are characteristically short segment but can be confluent when multiple. Postcontrast MRI can be particularly helpful, including when attempting to differentiate the long-segment myelopathy of neurosarcoidosis and aquaporin-4 (AQP4)-IgG–seropositive neuromyelitis optica spectrum disorder (NMOSD) and when characterizing spinal cord tumors such as primary neoplasms and metastases. Spinal dural arteriovenous fistula is another do-not-miss diagnosis, with characteristic MRI features both precontrast and postcontrast. Tract-specific white matter involvement can be a clue for diseases such as subacute combined degeneration, paraneoplastic myelopathy, and radiation myelitis, whereas gray matter–specific involvement can suggest conditions such as cord infarct, viral myelitis, or myelin oligodendrocyte glycoprotein (MOG)-IgG associated disorder.**

SUMMARY: **Knowledge of the neuroimaging findings of the many causes of spinal cord and cauda equina dysfunction is critical for both neurologists and neuroradiologists. A structured approach to lesion compartmental location and imaging feature characterization is recommended.**

CITE AS:
CONTINUUM (MINNEAP MINN) 2021;27(1, SPINAL CORD DISORDERS): 225–263.

Address correspondence to Dr Felix E. Diehn, Department of Radiology, Division of Neuroradiology, 200 First St SW, Rochester, MN 55905, diehn.felix@mayo.edu.

RELATIONSHIP DISCLOSURE:
Dr Diehn has received personal compensation for travel expenses for speaking engagements from the American Academy of Neurology, the American Academy of Pain Medicine, Mayo Clinic Department of Radiology, and the Spine Intervention Society. Dr Krecke reports no disclosure.

UNLABELED USE OF PRODUCTS/INVESTIGATIONAL USE DISCLOSURE:
Drs Diehn and Krecke report no disclosures.

INTRODUCTION

In patients with myelopathy, spinal cord signal abnormality on MRI, particularly increased T2 signal, can occur with a wide variety of diseases intrinsic and extrinsic to the spinal cord. To arrive at a specific diagnosis for such myelopathic signal abnormality or a limited imaging differential diagnosis, additional clinical and imaging features must be evaluated. The preceding articles in this issue detail many of the clinical considerations and therefore these are not further discussed here. Such additional imaging features include, but are not limited to, the cross-sectional pattern of involvement, the longitudinal extent, cord expansion, associated findings in the spinal cord, enhancement, any extrinsic compressive/adhesive cause of myelopathic signal, and findings outside the spinal canal. A complete workup that includes MRI can more often than not provide a specific diagnosis for a patient's myelopathy.[1] The wastebasket term *idiopathic transverse myelitis*, which is a diagnosis of exclusion, should generally not be used in MRI interpretations at primary presentation.[2] This article focuses on causes of myelopathy for which advanced imaging (particularly MRI but also CT or CT myelography) can provide specific diagnoses or short lists of differential considerations.

Select extrinsic causes of myelopathy are discussed first, since compression of the cord/cauda equina is more common than intrinsic myelopathy and the imaging findings can often specifically identify the disease process. This is followed by a discussion of intrinsic cord diseases. Because of space constraints, acute traumatic myelopathy (eg, fractures, traumatic malalignment, traumatic disk herniations, cord contusion/hemorrhage) is not considered specifically herein, nor are neurodegenerative/hereditary myelopathies. The brain MRI findings that can help diagnose diseases such as multiple sclerosis (MS) are also not included.

SPINAL CORD IMAGING BASICS

MRI is the principal modality for anatomic evaluation of the spinal cord and canal (TABLE 10-1[3]). The ability of MRI to noninvasively demonstrate and differentiate structures of the extradural, intradural-extramedullary, and intramedullary compartments in multiple anatomic planes is unparalleled. Radiographs, CT, CT myelography, conventional angiography, and CT angiography have more limited applications. CT of the spine is the modality of choice for trauma settings because of speed of acquisition and wide availability. As a first-line modality, the fundamental magnetic and radiofrequency environment of MRI systems is relatively inhospitable to the patient who is acutely traumatized, the necessary support devices, and personnel. Patients presenting with myelopathy may be intolerant of or unsafe for the MRI environment because of claustrophobia, body habitus, or critical medical devices. CT myelography can be a robust technique in these patients.

The standard MRI protocol of the spine relies on T1-weighted and T2-weighted sequences (TABLE 10-2) (FIGURE 10-1). Together, they produce outstanding evaluation of the extradural and intradural-extramedullary spaces. Higher sensitivity evaluation of the cord parenchyma is achieved by adding a sagittal T2-weighted short tau inversion recovery (STIR) sequence optimized to cord signal abnormality (inversion time of approximately 110 ms to 130 ms) rather than bone or paraspinal signal abnormality (inversion time of

Utility of Various Advanced Spinal Imaging Modalities in Evaluating the Spinal Cord

TABLE 10-1

Modality	Clinical scenario	Comments
MRI	First line for any suspected nontraumatic myelopathy; follow-up of most myelopathies; in acute traumatic myelopathy after initial evaluation with CT to assist in spinal canal evaluation and potential operative planning	For initial complete evaluation of a myelopathy or suspected/known infection/active inflammation/neoplasm/vascular cause, should be performed without and with IV gadolinium; include segments of spine clinically affected; protocol used depends on indication (refer to TABLE 10-2)
Magnetic resonance angiography (MRA)	Suspected or known vascular myelopathy; workup of myelopathy demonstrated on MRI of unknown cause; arterial dissection (including vertebral artery)	Typically performed with IV gadolinium; not a substitute for conventional angiography but can help guide spinal angiography if suggests level of dural arteriovenous fistula; CT angiography is an infrequently used alternative, especially if patient not an MRI candidate or MRI is not available; CT angiography is first line for acute arterial injury
CT	Acute trauma; assess for degree of calcification/ossification of a compressive lesion, degree of osseous stenosis; reasonable first-line examination (over CT myelography) if patient not an MRI candidate or MRI is not available; assess margins/nature of osseous lesions causing compressive myelopathy seen on MRI	Soft tissue attenuation lesions in the canal may be difficult/impossible to discriminate from CSF/cord
Conventional myelography and postmyelography CT	Patient not an MRI candidate or MRI is not available (including when CT has not diagnosed the cause of a myelopathy); surgical planning or problem solving; differentiation of arachnoid cyst, arachnoid web, and spinal cord herniation; assess dynamic nature of lumbar spinal stenosis with standing cone-beam technique	Minimally invasive; dynamic capabilities (temporal: initial contrast flow at level of a space-occupying lesion; positional: lateral decubitus, prone); other uses include evaluation of spontaneous intracranial hypotension/CSF leak (usually not in a setting of myelopathy)
Conventional angiography	Dural arteriovenous fistula (localizing level and, in appropriate cases, treatment); other spinal vascular malformation, including arteriovenous malformation; spinal vasculitis; localize artery of Adamkiewicz	Minimally invasive; MRA can inform search for fistula and decrease time/radiation dose; complete examination is from vertebral to internal iliac arteries; CT angiography is an alternative for artery of Adamkiewicz localization
Fludeoxyglucose positron emission tomography (FDG-PET) CT	Not typically used primarily for myelopathy but most commonly for metastatic workup of many suspected/known malignancies	Spinal canal a relative blind spot; normal variant increased uptake of conus; both neoplastic and, less commonly, inflammatory causes may show increased uptake[3]

CSF = cerebrospinal fluid; CT = computed tomography; IV = intravenous; MRI = magnetic resonance imaging.

approximately 150 ms to 170 ms). Axial plane imaging of cord and canal is most effective using T2-weighted techniques. Cord gray-white differentiation is best appreciated on axial images, with the gray matter expected to be slightly more hyperintense than the white matter. An axial gradient recalled echo (GRE) sequence can demonstrate the gray-white differentiation to better advantage than T2-weighted images; the inherently normal gray matter hyperintensity on this sequence relative to white matter should not be mistaken for abnormal. GRE sequences also have fewer CSF flow artifacts. Together and in conjunction with sagittal sequences, the two axial sequences can be complementary in evaluating intradural anatomy and pathology. IV administration of gadolinium with postcontrast T1-weighted imaging performed in at least the sagittal plane, if not also the axial plane, is recommended for complete evaluation of suspected intrinsic myelopathy with blood–spinal cord barrier breakdown (eg, infectious, active inflammatory, vascular, or neoplastic causes). Inclusion of diffusion-weighted imaging (DWI) in the MRI protocol is suggested for any hyperacute or acute myelopathy, particularly to help assess for infarct.[4]

CT myelography involves percutaneous intrathecal access and injection of iodinated contrast material, typically via lumbar puncture with fluoroscopic

TABLE 10-2 **MRI Protocols for Nontraumatic Myelopathy**

Indication	Tailored MRI protocol
Nontraumatic	Basic protocol: Sagittal: T1-weighted; T2-weighted; short tau inversion recovery (STIR) optimized for cord signal abnormality or proton density[a] (myelopathy sequence); with or without T2-weighted fat-suppressed sequence (STIR or fat saturation), especially if axial pain is present, as this helps evaluate for edema-type signal abnormality in bones/paraspinal soft tissues Axial: T2-weighted; with or without gradient recalled echo (GRE)[a] Initial complete evaluation includes postgadolinium sagittal with or without axial T1-weighted (fat suppression is based on radiologist preference, but strictly speaking not needed for intramedullary disease)[a]
Vascular	Basic protocol as above, including gadolinium; diffusion-weighted imaging if hyperacute/acute[a]; magnetic resonance angiography (MRA)[a]; consider thin-section heavily T2-weighted three-dimensional GRE steady state sequences[b] for dural arteriovenous fistula; consider GRE (sagittal with or without axial) for blood products
Neoplasm, infection, active inflammation	Basic protocol as above, including gadolinium; sagittal with or without axial T2-weighted fat-suppressed sequence (STIR or fat saturation)[a]; include fat saturation on postgadolinium T1-weighted images in at least one plane (sagittal or axial); consider diffusion-weighted imaging[a] if abscess suspected
Spinal cord herniation, arachnoid cyst, arachnoid web	Basic protocol as above; consider thin-section heavily T2-weighted three-dimensional GRE steady state sequences[b]
Scoliosis	Basic protocol as above; consider coronal plane (T2-weighted with or without T1-weighted)

MRI = magnetic resonance imaging.
[a] Sequences that ordering clinicians may want to specifically ask for in MRI request to ensure they are included.
[b] Examples include fast imaging employing steady state acquisition (FIESTA) and constructive interference in steady state (CISS).

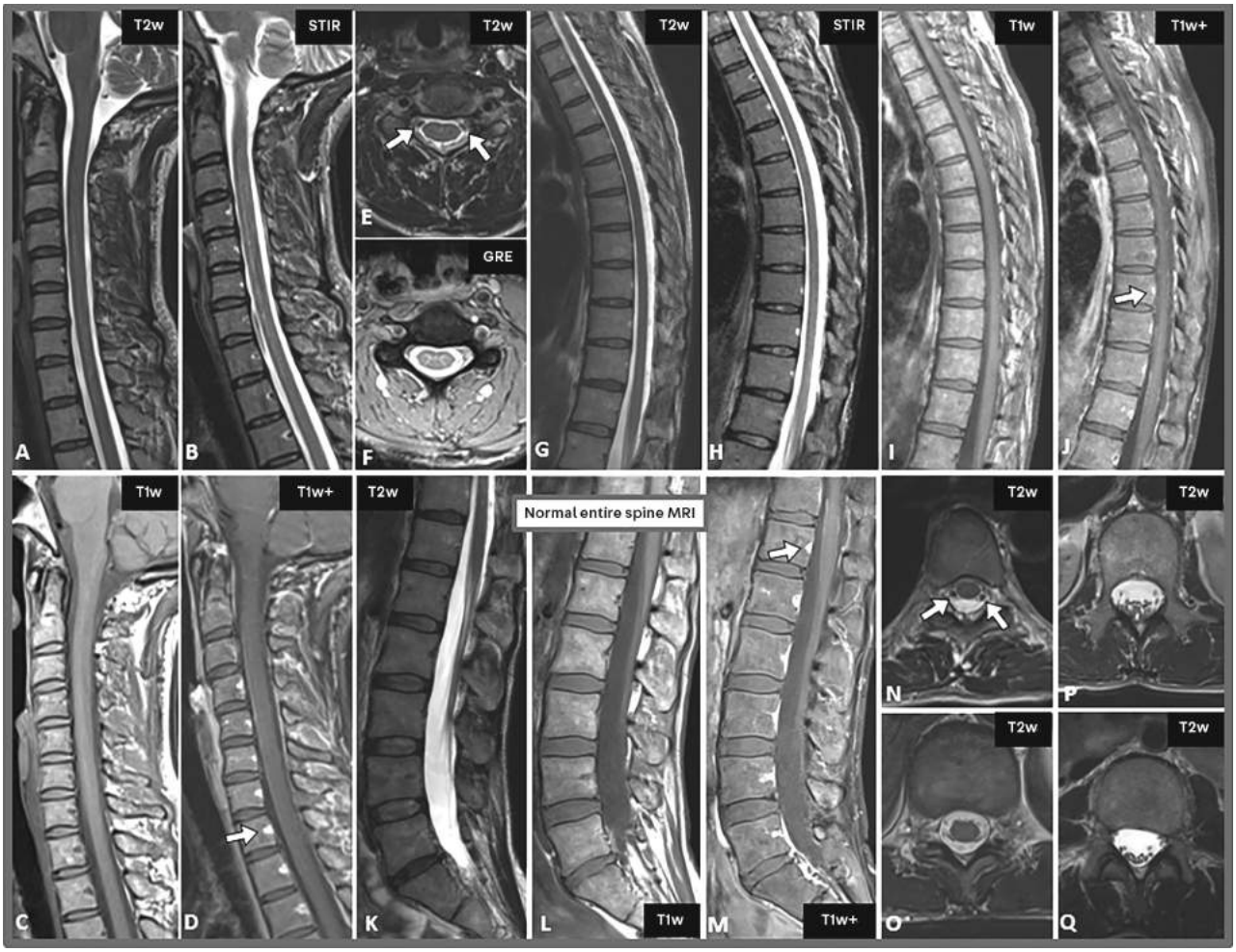

FIGURE 10-1

Normal spinal cord and cauda equina. Multiplanar multisequence images of the cervical (*A* through *F*), thoracic (*G* through *J, N, O*), and lumbar (*K* through *M*, *P*, *Q*) spine. The spinal cord contour is smooth throughout. The signal intensity of the spinal cord is relatively homogeneous, especially on sagittal images. Sagittal short tau inversion recovery (STIR) sequences optimized to detect spinal cord signal abnormality (cervical, *B*; thoracic, *H*) demonstrate mild normal T2 hyperintensity of cord gray matter more so than standard T2-weighted images. Gray-white differentiation is better appreciated on axial gradient recalled echo (GRE) (*F*) than conventional T2-weighted (*E*) images; the former are most useful in the cervical spine. CSF flow voids are more evident on axial T2-weighted (*E*, *N*, *arrows*) than GRE (*F*) images. Postcontrast, the basivertebral plexus accumulates gadolinium (*D*, *J*, *M*, *arrows*) and thus enhances compared to unenhanced T1-weighted images (*C*, *I*, *L*). The spinal cord expands slightly at the conus (sagittals *G* through *J*, *K* through *M*; axials *O*). The tip of the conus is normally above the L2-L3 interspace level; in this patient, it is at L1 (*P*). The cauda equina nerve roots are anatomically distributed and layer dependently posteriorly within the thecal sac in this supine patient (*K*, *P, Q*); they do not normally demonstrate appreciable enhancement (*M*). Fat suppression was employed on the postcontrast lumbar spine sagittal T1-weighted images but is not specifically necessary when evaluating the spinal cord and cauda equina.

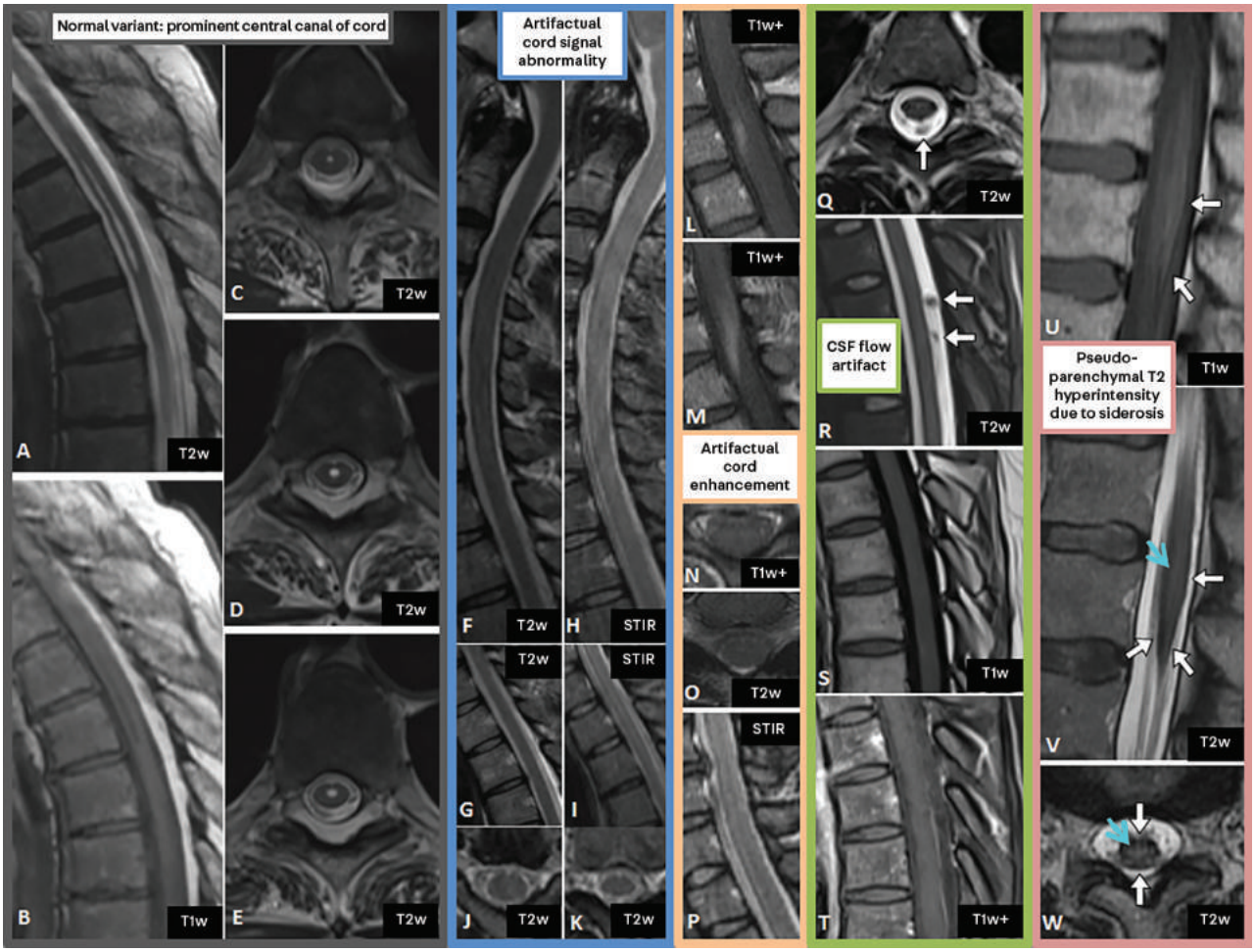

FIGURE 10-2

Normal variant and artifacts of the spinal cord. The central canal of the spinal cord is an ependyma-lined CSF space that can be mildly prominent as an anatomic variant (*A* through *E*); this is not a pathologic syrinx. Artifactual spinal cord signal abnormality (*F* through *K*) can occur for a variety of reasons, such as patient motion (eg, respiration, swallowing); it is usually more apparent on short tau inversion recovery (STIR) (*H*, *I*) than on conventional T2-weighted images (*F*, *G*). Evaluation of the spinal cord in two planes is essential; axial images (*J*, *K*) in this patient do not confirm the apparent T2 hyperintensity seen on sagittal images. Artifactual cord enhancement (*L* through *N*) can occur for similar reasons. Often, it is seen only in one of the two planes (seen sagittally in *L* and *M* but not axially in *N*, and no corresponding cord T2 hyperintensity is seen [*O*, *P*]). CSF flow artifact (*Q*, *R*) can simulate intrathecal pathology to the uninitiated; it is most apparent on conventional T2-weighted images (*Q*, *R, arrows*), and in this patient was misconstrued as nodular drop metastases. Note that it is not evident on the T1-weighted image (*S*) and does not enhance (*T*). In patients with chronic repetitive subarachnoid hemorrhage resulting in superficial siderosis, the low-signal-intensity hemosiderin that coats the pial surface of the spinal cord and conus (*U* through *W, white arrows*) can cause an artifact of pseudoparenchymal T2 hyperintensity (*blue arrows*, *V*, *W*).

guidance. Although myelography has decreased in popularity over the years, it is a low-risk technique for evaluating myelopathy in patients poorly suited for MRI, for surgical planning, and for problem solving, including for clarifying the differential diagnosis of arachnoid cyst, arachnoid web, and idiopathic spinal cord herniation. Myelography can also allow real-time observation of CSF dynamics and tailored patient positioning.

Normal Anatomy and Anatomic Variants

A slight expansion of the cord is evident in the cervical-thoracic region, from approximately C3 through T2. The thoracolumbar region of the spinal cord also expands slightly from approximately T9 through T12 before it progresses inferiorly to form the conus. These normal expansions may be missing in the pathologically atrophic cord, which is a nonspecific morphology that can be short or long segment. Cord atrophy can result from essentially any chronic or treated cause of myelopathy as well as from hereditary/neurodegenerative myelopathies.

The conus is normally located no lower than L2-L3. An ependyma-lined central canal is located within the spinal cord. This extends from the inferior aspect of the fourth ventricle to the tip of the conus, where it slightly dilates transiently during childhood into the normal ventriculus terminalis (the so-called fifth ventricle), which is rarely seen in adults. The central canal can be physiologically prominent and thereby evident as a normal variant on MRI; this is thin, usually only a few millimeters in diameter, and should not be confused with a syrinx (FIGURE 10-2). A syrinx (syringohydromyelia) is pathologic fluid within the spinal cord (central canal or parenchyma) and can have a wide variety of causes; when encountered for the first time, this finding should be evaluated with MRI without and with contrast to exclude a neoplastic cause. Findings that suggest a syrinx over a physiologically prominent central canal include a beaded appearance, eccentric location, cord enlargement, surrounding T2 hyperintensity, and an associated solid mass or enhancement.

For a complete discussion of the anatomy of the spinal cord, refer to the article "Spinal Cord Anatomy and Localization" by Todd A. Hardy, PhD, MBBS, FRACP,[5] in this issue of *Continuum*.

Pitfalls

A few pitfalls regarding the use of MRI for myelopathy deserve specific mention. The normal gray matter is slightly more hyperintense than the white matter, which may simulate abnormal T2 hyperintensity anteriorly and centrally on sagittal T2-weighted images (FIGURE 10-1). Second, patient motion can cause apparent but artifactual signal abnormality, including false-positive T2 hyperintensity in the cord (FIGURE 10-2). Third, adjacent to the cord, CSF flow artifact can confound; it can be particularly prominent on conventional T2-weighted images (FIGURE 10-2). Especially on axial images, this artifactual T2 hypointensity can simulate extradural or intradural lesions such as disk herniations, osteophytes, or nerve sheath tumors. As artifact, it often cannot be confirmed as truly lesional on sagittal images or other sequences. Axial GRE images are less susceptible to such motion artifact and can help problem solve. Fourth, chronic repetitive subarachnoid hemorrhage can result in superficial siderosis. In this condition, the T2-hypointense hemosiderin that coats the spinal cord can cause the parenchyma to appear relatively T2 hyperintense

KEY POINTS

- IV administration of gadolinium with postcontrast T1-weighted imaging performed in at least the sagittal plane, if not also the axial plane, is recommended for complete evaluation of suspected intrinsic myelopathy with blood–spinal cord barrier breakdown.
- Inclusion of diffusion-weighted imaging in the MRI protocol is suggested for any hyperacute or acute myelopathy, particularly to help assess for infarct.
- The central canal can be physiologically prominent and thereby evident as a normal variant on MRI; this is thin, usually only a few millimeters in diameter, and should not be confused with a syrinx.
- The normal gray matter is slightly more hyperintense than the white matter, which may simulate abnormal T2 hyperintensity anteriorly and centrally on sagittal T2-weighted images.

(pseudomyelopathic signal abnormality) (FIGURE 10-2). Finally, contrast-enhanced features are critical for correctly diagnosing a myelopathy (TABLE 10-3). However, apparent enhancement on postcontrast T1-weighted images is not always true enhancement. Precontrast images should always be reviewed for inherently T1-hyperintense substances (such as blood products) that can simulate enhancement on postgadolinium images.

COMPARTMENT APPROACH TO MYELOPATHY

The spinal canal can be divided into the extradural, intradural-extramedullary, and intramedullary compartments. Each compartment contains unique anatomic and histologic structures, greatly informing and simplifying the differential diagnosis of lesions in each compartment (FIGURE 10-3). Extrinsic causes of myelopathy or cauda equina symptoms can occur in the intradural-extramedullary and extradural compartments. The intramedullary compartment includes the parenchyma (spinal cord and conus).

Extradural Compartment

A wide variety of spinal or paraspinal lesions, both benign and malignant, may cause myelopathy or cauda equina symptoms by compression of neural tissue. Selected causes that are important to recognize are discussed here.

DISK HERNIATIONS. The most common mass in the epidural space is a disk herniation. Most disk herniations are located in the ventral/ventrolateral epidural space and remain in anatomic continuity with their parent disk, a key clue to the diagnosis. The disk herniation, especially when acute/subacute, may not have the same signal characteristics as the parent disk, which can cause confusion. Less commonly encountered locations for disk herniations that can compress neural tissue include the lateral/dorsal epidural space and the intradural compartment (FIGURE 10-4).[6] A highly prevalent finding for dorsal disk herniations is that the abnormal epidural soft tissue still typically maintains continuity with the parent disk in the ventrolateral epidural space, wrapping around the thecal sac dorsally.[7] Because of a lack of familiarity with this less commonly encountered location of disk herniation and given the often-acute clinical presentation with cauda equina syndrome, such dorsal herniations are frequently initially misdiagnosed as epidural hematomas, epidural abscesses, or synovial cysts. Misdiagnosis occurs in part because any of these lesions, including disk herniations, can and often do demonstrate peripheral enhancement. Peripheral enhancement is expected for disk herniations because of the surrounding inflammatory/fibrotic reaction. It is also the rule for synovial cysts and epidural abscesses (FIGURE 10-4). An additional uncommon location for disk herniations is the intradural compartment (FIGURE 10-4). In the lumbar spine, occasionally the dorsal edge of an intradural disk herniation may demonstrate a sharp posterior edge, the so-called hawk-beak sign.[8] Although disk herniations in the thoracic spine are commonly asymptomatic, they have a propensity to calcify, especially when giant. Such giant calcified disk herniations have a tendency to erode the dura and be intradural.[6] The calcified nature of a disk herniation is most easily appreciated on CT; on MRI, this often manifests as very low signal on T1-weighted and T2-weighted images. A clue to the diagnosis of any disk herniation is air within the lesion (ie, the vacuum phenomenon) due to accumulation of nitrogen gas.

SYNOVIAL CYSTS. The spectrum of posterior element spondylotic changes includes synovial cysts (also known as facet joint cysts), which are most common in the lumbar spine, particularly at L4-L5. Although most such synovial cysts are small and asymptomatic and often even external to the spinal canal,[9] some can impair the traversing cauda equina nerve roots as the cysts project typically anteromedially from the facet joint into the spinal canal (FIGURE 10-4). Anatomic continuity with the adjacent arthropathic facet joint in at least one plane allows confident diagnosis on MRI but is not always identifiable. Additional clues to the diagnosis are arthropathy of the adjacent facet joint, including increased fluid within the joint; characteristic location laterally within the spinal canal, including in the lateral recess (although other locations, including foraminal and dorsal midline, also occur); fluidlike or heterogeneous internal signal intensity of the cyst; and a sometimes relatively thick and T2-hypointense rim that typically enhances after contrast (FIGURE 10-4). The heterogeneous internal signal characteristics of synovial cysts are wide-ranging and include T1 and T2 hypointensity or hyperintensity or a combination. CT can more readily identify the calcification that synovial cysts may harbor in their wall or internally.

EXTRADURAL HEMATOMAS AND ABSCESSES. Extradural hematomas and abscesses are more commonly epidural than subdural. A history of trauma, spinal procedure/surgery, or anticoagulated/coagulopathic state can be a helpful clue to the diagnosis of extradural hematoma. The signal characteristics of spinal hematomas can be quite variable because of the inherently complex signal of blood products and the varying possible and potentially mixed age contents of such collections.[10]

Confident diagnosis of an extradural abscess can be aided by symptoms, signs, and laboratory markers of infection. MRI of extradural abscesses may show associated adjacent inflammatory changes, including in the paraspinal soft tissues and bones, or frank findings of spondylodiskitis (FIGURE 10-4).[11] The inflammatory changes, phlegmon, or abscess are often best visualized on images with fat suppression, which are critical sequences in this setting. On T2-weighted fat-suppressed images, hyperintensity is expected, and on postgadolinium T1-weighted fat-suppressed images, enhancement will be present. Extradural abscesses should enhance peripherally, with central fluidlike T2-hyperintense and T1-hypointense contents (FIGURE 10-4).

OSSIFICATION OF THE POSTERIOR LONGITUDINAL LIGAMENT. Ossification of the posterior longitudinal ligament may cause compression of the spinal cord, alone or in combination with spondylotic changes (FIGURE 10-5). It is implicated in up to one-fourth of cases of cervical myelopathy and is most common in the cervical spine.[12] On CT, ossification of the posterior longitudinal ligament is readily identifiable as flowing ossification along the expected course of the posterior longitudinal ligament in and along the midline at the ventral aspect of the spinal canal. Like diskal calcifications or marginal osteophytes, the ossification can be limited to disk space/endplate levels. However, it is also typically continuous and located posterior to vertebral bodies. On axial images, particularly on CT, characteristic inverted T morphology may be identified. Because of its dense osseous nature, when mature, ossification of the posterior longitudinal ligament signals hypointense on T1-weighted and T2-weighted images and does not enhance; the hypointensity becomes more prominent on GRE images (called

KEY POINTS

- The most common mass in the epidural space is a disk herniation. Most disk herniations are located in the ventral/ventrolateral epidural space and remain in anatomic continuity with their parent disk, a key clue to the diagnosis.
- A highly prevalent finding for dorsal disk herniations is that the abnormal epidural soft tissue still typically maintains continuity with the parent disk in the ventrolateral epidural space, wrapping around the thecal sac dorsally.
- The heterogeneous internal signal characteristics of synovial cysts are wide-ranging and include T1 and T2 hypointensity or hyperintensity or a combination.
- MRI of extradural abscesses may show associated adjacent inflammatory changes, including in the paraspinal soft tissues and bones, or frank findings of spondylodiskitis.
- On CT, ossification of the posterior longitudinal ligament is readily identifiable as flowing ossification along the expected course of the posterior longitudinal ligament in and along the midline at the ventral aspect of the spinal canal.

TABLE 10-3 **Specific Enhancement Findings in the Diagnosis of T2-hyperintense Spinal Cord Lesions**[a]

Disease	Enhancement findings postgadolinium	Other key helpful MRI findings
Extradural		
Cervical spondylotic (compressive) (FIGURES 10-5G through 10-5R)	Pancakelike on sagittal, at/just below maximal stenosis, within larger region of increased T2 signal; often peripheral on axial, sparing gray matter	Spondylotic changes causing cord compression, which may be greatest in extension
Disk herniation (FIGURES 10-4A through 10-4Q); synovial cyst (FIGURES 10-4R through 10-4W); epidural or subdural hematoma or abscess (FIGURES 10-4X through 10-4AA)	Peripheral enhancement expected for these lesions (acute hematoma usually does not enhance)	Disk herniation: usually ventral epidural but can be lateral/dorsal, rarely intradural Synovial cyst: may have complex internal signal with or without T2-hypointense rim Abscess: usually has associated inflammatory changes elsewhere, such as in bone/disks (osteomyelitis-diskitis) and paraspinal regions
Hirayama disease (FIGURES 10-7G through 10-7R)	Robust enhancement of the enlarged dorsal epidural space on flexion	Loss of cervical kyphosis, loss of dural attachment, asymmetric cord atrophy/flattening, focal myelomalacia
Intrinsic: neoplastic-primary		
Ependymoma (FIGURES 10-11A through 10-11I)	Typically present, well-defined	Central location, relatively well defined, cystic change, cap sign (polar hemorrhage)
Astrocytoma (FIGURES 10-11J through 10-11P)	Usually present but may not be; may be patchy/ill-defined/subtle	Eccentric location, relatively poorly defined, can be holocord
Hemangioblastoma (FIGURES 10-11Q through 10-11V)	Avidly enhancing nodule on cord surface, often dorsally	With or without cyst, with significant cord edema/syrinx for lesion size; if von Hippel-Lindau disease, often multiple, with or without lesions in posterior fossa, with or without cysts/neoplasms in pancreas, kidneys, adrenal glands
Intrinsic: neoplastic-secondary		
Metastasis (FIGURES 10-11W through 10-11BB)	Rim, flame, and/or central dot signs	Significant cord edema for lesion size, evidence for other metastatic disease with or without primary tumor

CONTINUED ON PAGE 235

CONTINUED FROM PAGE 234

Disease	Enhancement findings postgadolinium	Other key helpful MRI findings
Intrinsic: demyelinating/immune-mediated/ inflammatory		
Multiple sclerosis	Enhancing lesion(s) when acute/ active; ill-defined, solid/nodular, ring, or partial ring	Small, peripheral, multiple; usually no cord enlargement
Aquaporin-4-IgG neuromyelitis optica spectrum disorder (NMOSD) (FIGURES 10-12H through 10-12T)	Ring/partial ring, of a long-segment myelopathy	Cervicomedullary junction involved; T1-hypointense components,T2-hyperintense spotty foci
Neurosarcoidosis (FIGURES 10-12U through 10-12EE)	Along dorsal subpial/pial aspect of a long-segment myelopathy; with or without extension into central canal (trident sign); may persist over months	With or without hilar/mediastinal adenopathy; with or without meningeal more than osseous lesions
Myelin oligodendrocyte glycoprotein (MOG)-IgG–associated myelitis (FIGURES 10-12FF through 10-12KK)	Lacking or mild	Multiple longitudinally extensive lesions predominate; T2 hyperintensity confined to gray matter; thoracolumbar
Paraneoplastic (FIGURES 10-13I through 10-13N)	Tract-specific when present	Long segment; evidence for primary tumor with or without metastatic disease
Intrinsic: vascular		
Infarct (FIGURES 10-14A through 10-14L)	Anterior cord/central gray if anterior spinal artery infarct; associated bone infarcts typically enhance, and cauda equina may enhance (both usually in subacute phase)	Restricted diffusion when acute
Dural arteriovenous fistula (FIGURES 10-14M through 10-14V)	Vascular-type along conus/cord surface (serpiginous, corresponding to T2-hypointense flow voids); parenchyma may enhance, including missing piece sign	T2-hypointense flow voids along conus/cord surface; parenchymal T2-hyperintense signal sparing periphery
Cavernous malformation (FIGURES 10-14W through 10-14CC)	Minimal, if any (apparent enhancement may reflect inherent T1 hyperintensity)	Heterogeneity (blood products), including blooming on gradient recalled echo (GRE) imaging; edema if hemorrhage is acute/ subacute; blood products in adjacent spinal cord extending craniocaudally

IgG = immunoglobulin G.
[a] Many other causes of myelopathy can enhance, especially if in an acute/active phase, but variably so and without such relatively specific patterns.

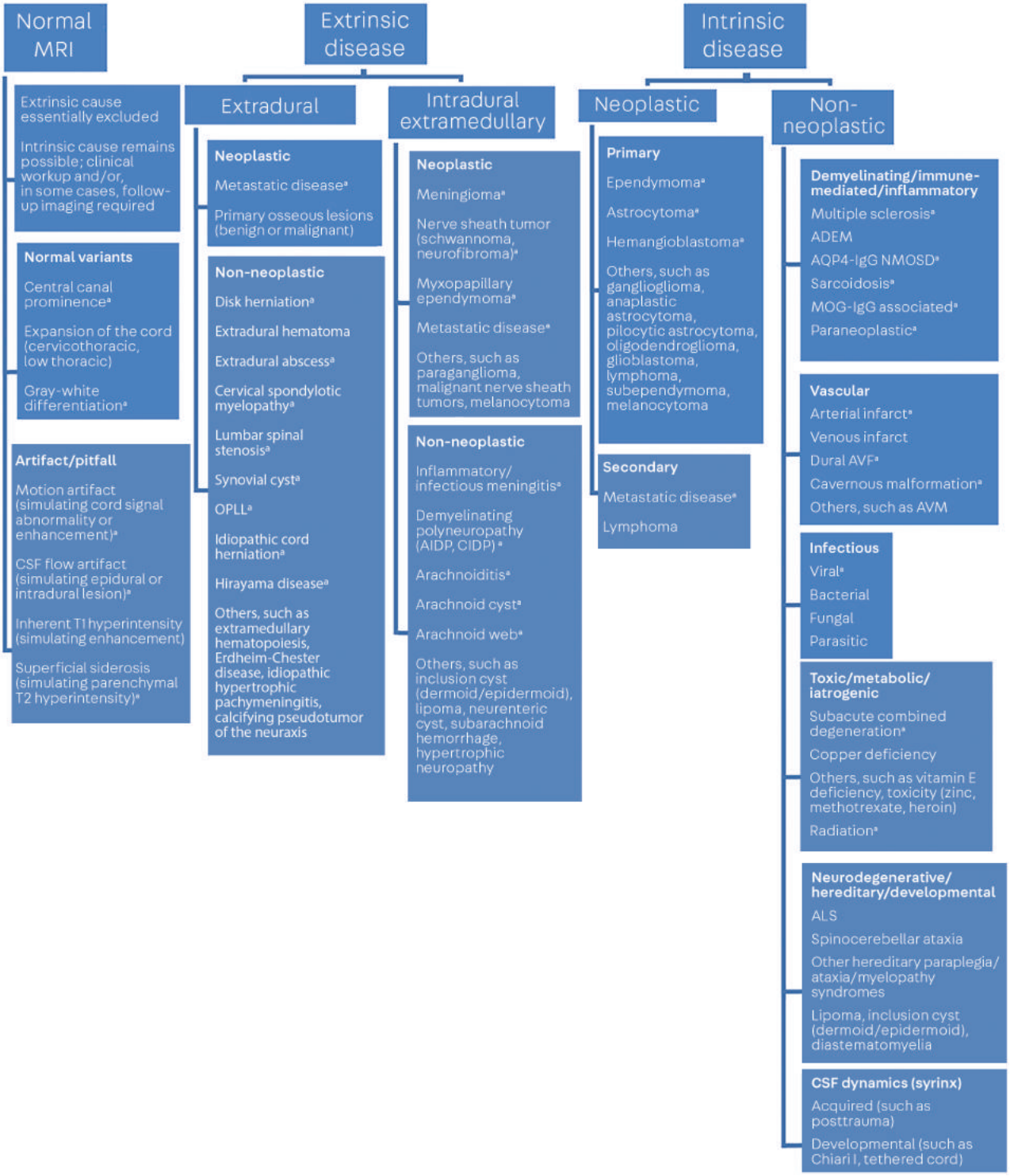

FIGURE 10-3

Causes of nontraumatic myelopathy identifiable on imaging, based on location and category.

ADEM = acute disseminated encephalomyelitis; AIDP = acute inflammatory demyelinating polyradiculoneuropathy; ALS = amyotrophic lateral sclerosis; AQP4 = aquaporin-4; AVF = arteriovenous fistula; AVM = arteriovenous malformation; CIDP = chronic inflammatory demyelinating polyradiculoneuropathy; CSF = cerebrospinal fluid; MOG = myelin oligodendrocyte glycoprotein; MRI = magnetic resonance imaging; NMOSD = neuromyelitis optica spectrum disorder; OPLL = ossification of the posterior longitudinal ligament.

[a] Discussed in detail and/or illustrated specifically in this article.

FIGURE 10-4

Disk herniations in unusual locations and other common peripherally enhancing extradural lesions. Dorsal disk herniations (*A* through *H*) can cause diagnostic uncertainty on imaging, even for neuroradiologists. A clue to a disk herniation in any location can be the presence of air within the lesion (*A*, *B, white arrows*); this is an extension of the intradiskal vacuum sign that occurs as a result of accumulation of nitrogen gas within a degenerated disk. When located in the dorsal epidural space, disk herniations (*A* through *H, white arrows*) tend to still demonstrate a connection with the parent disk in the ventral epidural space (*B, black arrow*; *C*, *D*, *H, blue arrows*). In this patient, the dorsal disk herniation migrates cranial and caudal to the parent L4-L5 interspace, and like disk herniations in any location, peripherally enhances (*G*, *H*). Intradural disk herniations (*I* through *Q, white arrows*) are uncommon. Air within the lesion (*P*, *Q*), peripheral enhancement (*K*, *N*), and continuity with adjacent parent disk material in the ventral epidural space can be clues to the diagnosis. CT myelography can be used to problem solve (*O*, *Q*), in this case confirming the diagnosis by demonstrating a partially air-containing intrathecal filling defect. Synovial cysts (*R* through *W, white arrows*) can have variable signal characteristics. The rim of the lesion may be T2 hypointense (*R*, *T, white arrows*), and this rim typically enhances (*V*, *W, white arrows*). Connection to or at least continuity with an arthropathic facet joint (*T, blue arrow*) can be a helpful clue. Epidural abscesses (*X* through *AA*) (and subdural abscesses, *not shown*) also peripherally enhance (*Y*, *AA, white arrows*). The central aspect of the lesion should be T2 hyperintense (*X*) and T1 hypointense (*Y* through *AA*), owing to the purulent contents. Adjacent findings of spondylodiskitis, such as diskal T2 hyperintensity (*X, arrowhead*), vertebral body T2 hyperintensity, and contrast enhancement suggesting osteomyelitis (*X*, *Y, blue arrows*), can be helpful clues.

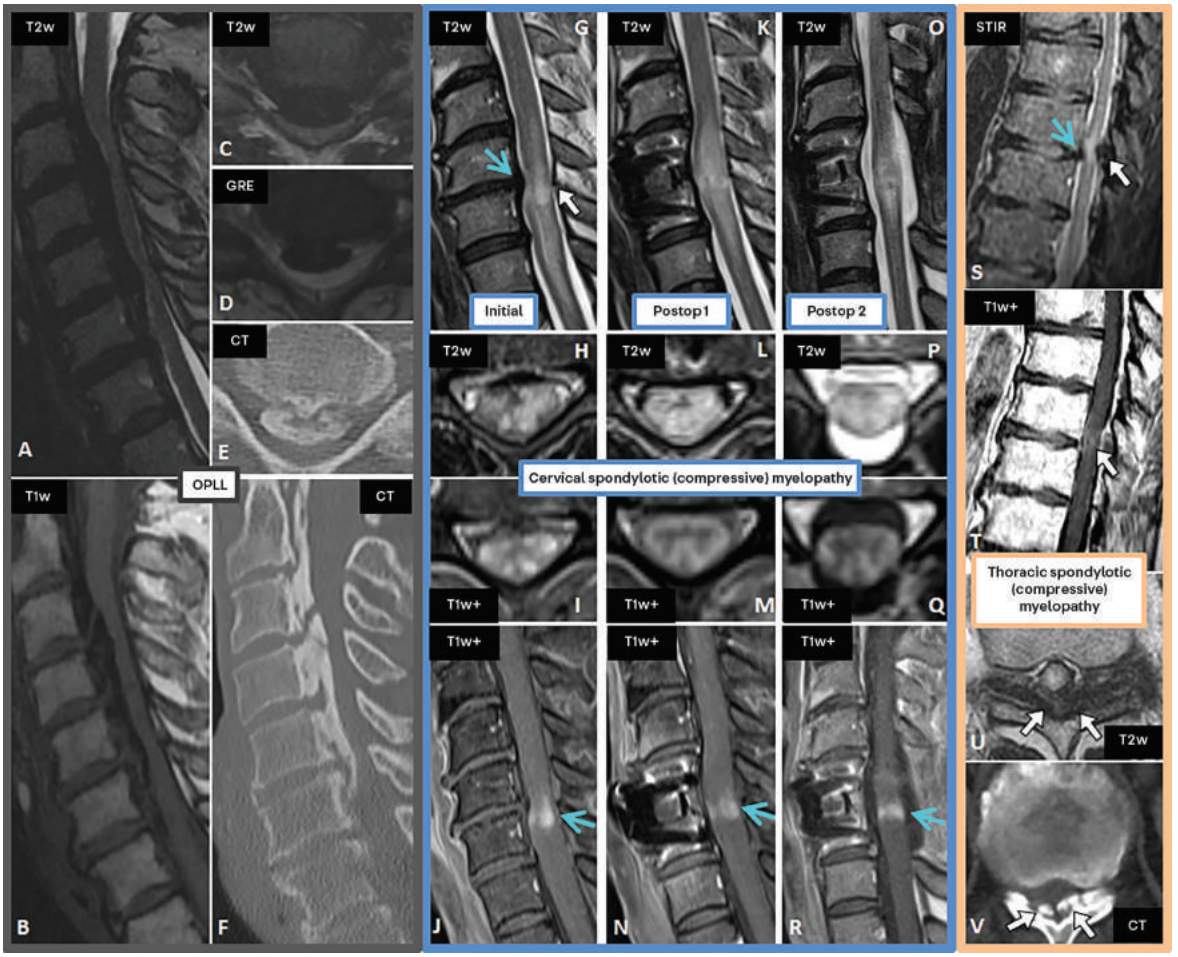

FIGURE 10-5

Extradural benign compressive cervical and thoracic myelopathy. Ossification of the posterior longitudinal ligament (*A* through *F*) can cause significant spinal cord compression even in the absence of appreciable spinal cord T2 hyperintensity (*A*, *C*, *D*). It can have variable signal characteristics, but most commonly mature bone signals hypointense on T2-weighted and T1-weighted images (*A* and *C*; *B*, respectively). Because of the osseous nature, the ossified ligament often appears more prominent on gradient recalled echo (GRE) imaging (*D*). CT can more definitely characterize this entity (*E*, *F*). The ossification involves not only disk space but also vertebral body levels, a finding that distinguishes it from disk-osteophyte complexes at interspace levels. Cervical spondylotic (compressive) myelopathy (*G* through *J*, *K* through *N*, *O* through *R*, three different MRI dates in the same patient) can present with characteristic imaging findings but may be confused with inflammatory/neoplastic myelopathy. On the initial sagittal T2-weighted image of this patient, the spinal cord compression is related to both anterior (*G, blue arrow*) and posterior (*G, white arrow*) spondylotic changes (ie, a disk osteophyte complex and ligamentum flavum redundancy, respectively). T2 hyperintensity of the spinal cord is longitudinal, spindle-shaped, and mildly expansile (*G*, *H*). A characteristic enhancement pattern features peripheral distribution (white matter involvement, sparing gray matter) in the axial plane (*I*) and pancakelike morphology at/just caudal to the cord compression in the sagittal plane (*J, white arrow*). After an anterior decompressive surgery, the findings persisted (*K* through *N*), as they may for months to even years, with the spinal cord mildly expanding into the more capacious canal. The patient underwent posterior decompressive surgery, and the characteristic findings again persisted (*O* through *R*), which is common. Thoracic spondylotic (compressive) myelopathy (*S* through *V*) occurs with lower frequency than its cervical counterpart; most spondylotic changes encountered in the thoracic spinal canal are asymptomatic. Findings can be similar, including cord compression from anteriorly or posteriorly (*S, blue arrow*; *S*, *U*, *V*, *white arrows,* respectively) and focal enhancement (*T, white arrow*).

blooming) (FIGURE 10-5). It can cause significant spinal cord compression, but owing to its slow chronic development, spinal cord T2 hyperintensity may be minimal or absent (FIGURE 10-5). Ossification of the posterior longitudinal ligament can be seen in association with diffuse idiopathic skeletal hyperostosis (DISH).[12] DISH is characterized primarily by ossification of the anterior longitudinal ligament along the ventral aspect of the spinal column, with relative disk space and facet joint preservation.

CERVICAL AND THORACIC SPONDYLOTIC MYELOPATHY. Cervical spondylotic myelopathy deserves special mention, especially given its characteristic but underrecognized pattern of spinal cord enhancement after gadolinium (FIGURE 10-5), which can be confused with inflammatory or neoplastic intrinsic myelopathy. The spondylotic compressive findings are those that typically narrow the spinal canal, any of which may be present: a developmentally narrow canal (short pedicles), spondylolisthesis, disk herniations, osteophytes, ossification of the posterior longitudinal ligament, and ligamentum flavum redundancy/ossification. The cord may be compressed ventrally or dorsally, or both (FIGURE 10-5). The nature of intramedullary signal abnormality, if present, has pathologic correlation. T2 hyperintensity is often longitudinal, spindle-shaped, and mildly expansile. This signal abnormality represents a range of reversible (eg, edema) and irreversible (eg, demyelination, gliosis, cystic necrosis) causes. When faint and indistinct, it more likely represents reversible edema. When very intense and well defined, it is more likely caused by fixed gliosis or cystic necrotic change. Similarly, intramedullary T1 hypointensity correlates with irreversible necrosis and myelomalacia.[12] Similar to a cord that has been previously acutely traumatized, T2 hyperintensity may be present cephalad to the cord compression in the posterior columns because of wallerian degeneration or caudal to the compression in the lateral columns because of corticospinal tract degeneration.

After gadolinium administration, T1-weighted images in cervical spondylotic myelopathy often demonstrate a characteristic narrow transverse (pancakelike) band of cord enhancement at or slightly caudal to the focus of spinal stenosis (FIGURE 10-5).[13,14] On axial images, the cross-sectional involvement of cord enhancement is variable, but it is often peripheral and limited to the white matter, either hemicord or bilateral. This enhancement, first reported in 2004,[15] occurs within the region of abnormal cord T2 hyperintensity; the latter is much greater in longitudinal extent. It often persists for a variable duration even after decompressive surgery (FIGURE 10-5).[14] Awareness of the enhancement pattern is critical for expedient diagnosis, treatment, and avoidance of unnecessary biopsy.[14] Of note, even in cases demonstrating intramedullary enhancement, the canal narrowing may not appear compressive in the recumbent neutral position. Additional sagittal sequences in passive extension and flexion may reveal compressive stenosis with extension and may more clearly show intrinsic cord T2 hyperintensity in flexion.[16] Findings on diffusion tensor imaging, a sophisticated MRI technique that is not yet routinely used clinically in most centers, may better correlate with clinical severity than standard techniques.[17]

Compressive myelopathy also occurs in the thoracic spine but with less frequency (FIGURE 10-5). A developmentally small spinal canal, degenerative hypertrophy of facet joints, ligamentum flavum redundancy/ossification, and large disk herniations can cause cord compression. Hypertrophy of facet joints

KEY POINT

- **After gadolinium administration, T1-weighted images in cervical spondylotic myelopathy often demonstrate a characteristic narrow transverse (pancakelike) band of cord enhancement at or slightly caudal to the focus of spinal stenosis.**

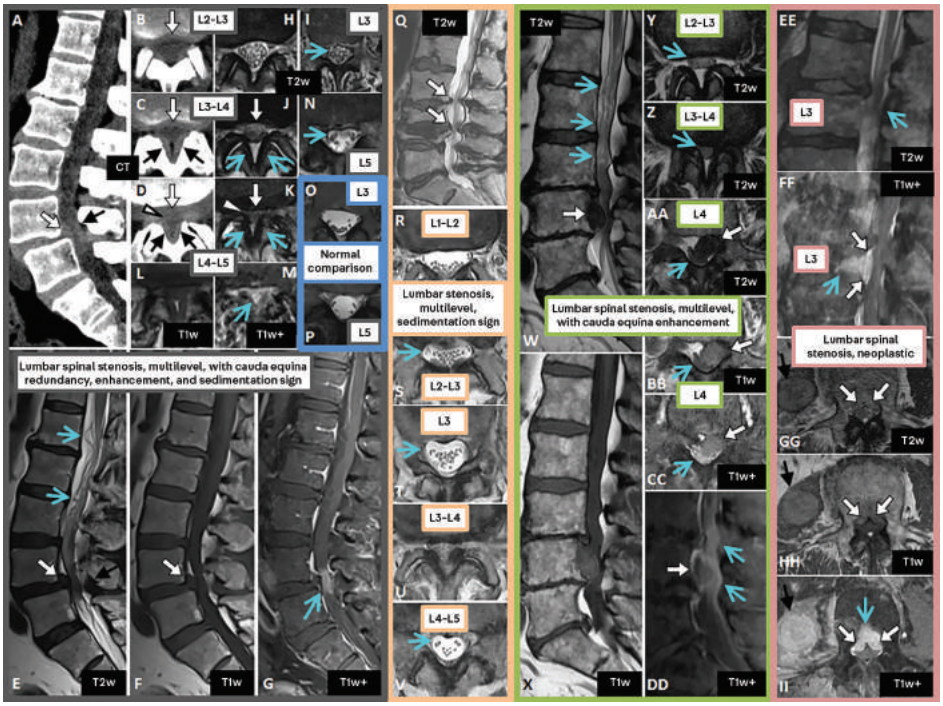

FIGURE 10-6

Lumbar spinal stenosis. Multilevel multifactorial lumbar spinal stenosis (*A* through *N*, *Q* through *V*, *W* through *DD*, three different patients) is common in patients who present with neurogenic intermittent claudication. In the first patient (*A* through *N*), unenhanced CT (*A* through *D*) demonstrates spinal stenosis, although MRI (*E* through *N*) displays the contributing findings and degree of narrowing to better advantage. In this patient, multifactorial spinal canal narrowing is mild at L2-L3 (*B*, *H*), moderate at L3-L4 (*C*, *J*), and advanced at L4-L5 (*D* through *G*, *K* through *M*). The stenosis has both ventral (*A* through *F*, *K, white arrows*) and dorsal components (*A*, *C* through *E, black arrows*; *J* through *K, blue arrows*). Ventrally, disk bulges contribute at L2-L3 through L4-L5, and at the latter, low-grade anterolisthesis also contributes. At the advanced L4-L5 stenosis, the CSF is nearly completely effaced (*D*, *K, arrowheads*) and the cauda equina focally enhances (*G*, *M, white arrows*). Because of the high-grade stenosis, the cauda equina nerve roots are redundant/tortuous in the sagittal plane (*E, blue arrows*) and abnormally ventrally located at several levels in the axial plane (sedimentation sign; *I* at L3, *N* at L5, *blue arrows*); a normal comparison at these levels is provided (*O*, *P*), demonstrating normally posteriorly dependently layering nerve roots. A companion case of multilevel, multifactorial lumbar stenosis (*Q* through *V*) demonstrates moderate spinal stenosis at L2-L3 and advanced stenosis at L3-L4 (*Q, white arrows*). At L2-L3, L3, and L4-L5, the nerve roots are located more ventrally than normal (*S*, *T*, *V*, *blue arrows,* respectively). At the high-grade L3-L4 stenosis (*U*), one cannot evaluate for the sedimentation sign. A second companion case of multilevel, multifactorial lumbar spinal stenosis (*W* through *DD*) also demonstrates cauda equina redundancy/tortuosity (*W, blue arrows*) and cauda equina enhancement greatest at the highest degree of narrowing (*CC*, *DD, blue arrows*). A developmentally narrow spinal canal contributes to the spinal stenosis. Superimposed spondylotic changes result in spinal stenosis that is moderate at L2-L3 (*Y, blue arrow*) and advanced at L3-L4 and L4 vertebral body levels (*Z*, *AA*, *blue arrows,* respectively). A large disk extrusion posterior to the L4 vertebral body primarily contributes to the spinal stenosis (*W*, *AA* through *DD, white arrows*); this peripherally enhances as can be expected (refer to FIGURE 10-4). Neoplastic spinal stenosis (*EE* through *II*) can also occur, especially with neoplastic involvement of the ventral epidural space (*FF* through *II, white arrows*), which in this patient contributes to relatively advanced spinal canal narrowing (*EE, blue arrow*). On axial images, the bilateral ventral epidural involvement with preservation of the midline septum (draped curtain sign, *GG* through *II, white arrows*) suggests an indolent process such as malignancy over a more rapidly aggressive process such as infection. In this patient, enhancing tumor involves the basivertebral vein (*FF*, *II, blue arrows*) and paraspinal metastatic disease is evident in the right retroperitoneal musculature (*GG* through *II, black arrows*).

can be especially subtle as the encroachment intrudes from the posterolateral aspects of the canal; thus, it is difficult to recognize in the sagittal plane due to volume averaging. These stenoses tend to occur in the upper thoracic levels or the region of the lumbar cord and conus medullaris.

LUMBAR SPINAL STENOSIS. Lumbar spinal stenosis is often a multifactorial and multilevel process (FIGURE 10-6). The compartments that may be involved include the thecal sac, the lateral recesses of the traversing nerve rootlets within the spinal canal, and the neural foramina. Similar to cervical spondylotic myelopathy, any or all of the following may be present: a developmentally narrow canal (short pedicles), spondylolisthesis, disk herniations, osteophytes, epidural lipomatosis, and ligamentum flavum redundancy/ossification or facet arthropathy. Synovial cysts associated with facet arthropathy are discussed separately above. Epidural lipomatosis can partially contribute to or primarily result in spinal stenosis; the diagnostic clues are relatively diffuse increase in the amount of epidural fat and a lack of normal segmentation of the dorsal epidural fat at the base of spinous processes. Lumbar spinal canal stenosis is often an incidental asymptomatic finding; this is a specificity flaw of imaging.[12] However, especially when at least moderate in degree, multicompartmental, or multilevel, lumbar spinal canal stenosis may impair the cauda equina nerve roots and result in neurogenic intermittent claudication.

Findings that suggest a relatively high grade and symptomatic lumbar stenosis include redundancy/tortuosity of the cauda equina nerve roots and the sedimentation sign (FIGURE 10-6). In the supine patient with no lumbar stenosis, cauda equina nerve roots layer dependently at the posterior aspect of the thecal sac. In patients in whom the course of the nerve roots is altered by spinal stenosis, the nerve roots fail to layer in such dependent fashion and are located ventrally in the thecal sac (the sedimentation sign).[18] Although large studies have not been performed, a 2019 meta-analysis of available literature suggests high sensitivity, specificity, and clinical diagnostic performance for this sign.[19] An additional associated finding that can cause confusion, analogous to cervical spondylotic myelopathy, is focal enhancement of the cauda equina nerve roots centered at the level of spinal canal stenosis (FIGURE 10-6). A shortcoming of standard imaging is the sensitivity flaw of trying to detect spinal stenosis in the relaxed supine patient. Imaging in an axial load-bearing position can accentuate or even reveal stenosis compared to supine examinations. Such imaging can be performed in the upright position, for example, with cone-beam CT myelography (FIGURE 10-7) or select MRI scanners (eg, 0.6T open upright systems), neither of which are in widespread use.

HIRAYAMA DISEASE. The purported pathophysiology of Hirayama disease (also known as monomelic amyotrophy) (FIGURE 10-7) is a short dura mater (relative to vertebral column length) that moves anteriorly during neck flexion and results in compression of the posterior aspect of the spinal cord. If Hirayama disease is suspected clinically or based on neutral position MRI, flexion MRI should be performed as it can demonstrate findings to better advantage and increase diagnostic confidence.[20,21] MRI may demonstrate loss of normal cervical lordosis in the neutral position, a finding that is not diagnostically specific. Asymmetric cord atrophy or flattening of the lower cervical/upper thoracic cord may also be present, often greatest at C6,[22] with

KEY POINTS

- Findings that suggest a relatively high grade and symptomatic lumbar stenosis include redundancy/tortuosity of the cauda equina nerve roots and the sedimentation sign.
- If Hirayama disease is suspected clinically or based on neutral position MRI, flexion MRI should be performed as it can demonstrate findings to better advantage and increase diagnostic confidence.

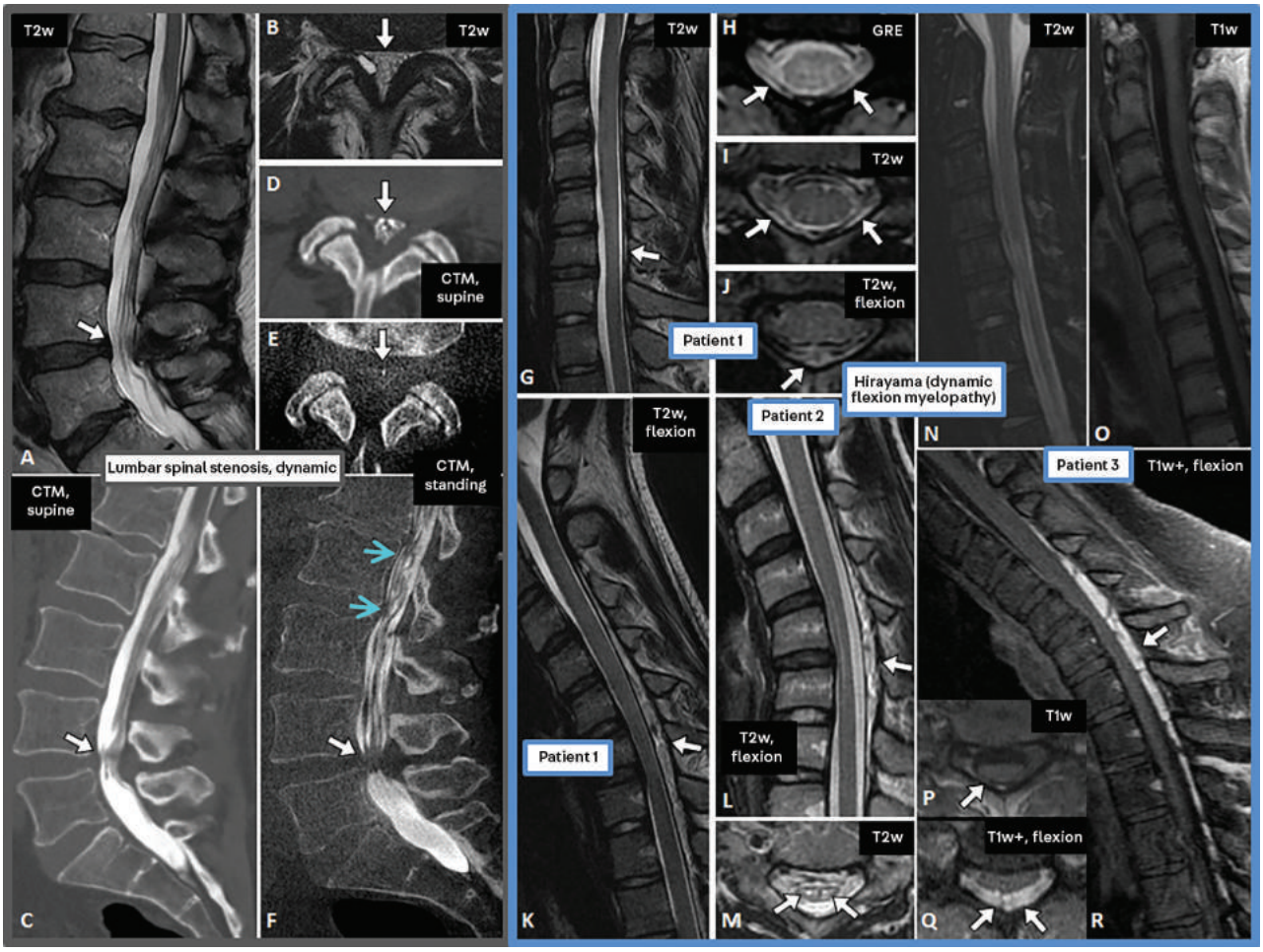

FIGURE 10-7

Dynamic lumbar and cervical spinal stenosis. Dynamic lumbar spinal stenosis (*A* through *F*) is not optimally imaged in routine supine MRI or CT/CT myelography. In this patient, such standard recumbent imaging demonstrates, at most, moderate spinal stenosis at L4-L5 (*A*, *B*, *white arrows*, MRI; *C*, *D*, CT myelography). A small right synovial cyst (*B*) contributes to the spinal canal narrowing. When the patient is imaged in the standing position of axial loading using cone-beam CT myelography, the degree of stenosis changes to advanced (*E*, *F*, *white arrows*) and the cauda equina becomes redundant/tortuous (*F, blue arrow*). Hirayama disease (*G* through *K*; *L*, *M*; *N* through *R*, three different patients) is a dynamic flexion myelopathy. On neutral images, loss of normal cervical lordosis (*G*) and loss of attachment of the dura to the lamina can be present; the latter best seen on axial images (*H* through *I, white arrows*). This loss of dural attachment on axial images may become more prominent in flexion (*J, white arrow*), and the dorsal epidural space can be seen to expand, especially on sagittal images in flexion (*K*, *R*) compared to neutral positioning (*G, white arrow*). This results in dynamic spinal canal narrowing and mass effect on the cord. In the first companion case (Patient 2) (*L*, *M*), the dorsal epidural space becomes prominent in flexion (*L, white arrow*; *neutral not shown*) and accompanying bilateral myelomalacia of the cord is seen (*M, white arrows*). A second companion case (Patient 3) (*N* through *R*) again demonstrates loss of cervical lordosis (*N*, *O*) and loss of dural attachment to the lamina axially (*P, white arrow*). Postcontrast and in flexion, compared to images in neutral positioning (*N* through *P*), the dorsal epidural space significantly enlarges, acts with mass effect on the spinal cord, and enhances robustly (*Q*, *R, white arrows*).

or without focal myelomalacia-type T2 hyperintensity. When present, the short-segment abnormal T2 hyperintensity in the focally atrophied cord primarily involves the bilateral anterior or anterior and lateral horns of the gray matter (the owl-eyes or snake-eyes sign, discussed further in the later section on spinal cord infarcts).[23] The posterior dura can be seen to be anteriorly displaced (loss of attachment to the adjacent lamina), a finding that can be present on neutral imaging[24] but for which flexion images increase confidence. This finding is associated with engorgement of the dorsal epidural venous plexus, which acts as an epidural mass, can cause cord flattening, and typically robustly enhances.[21,24]

OTHER EXTRADURAL CAUSES OF MYELOPATHY. The diagnoses discussed above are not all of the extradural causes of myelopathy or cauda equina impairment. Primary malignant and benign osseous lesions may grow into the spinal canal but are beyond the scope of this discussion. Metastatic disease and multiple myeloma, plasmacytoma, and lymphoma are commonly encountered and usually arise from the osseous components of the spine, including the vertebral body and posterior elements. Metastatic disease can also affect the epidural or, very rarely, subdural compartments; the former is commonly because of extension from adjacent osseous disease (FIGURE 10-6). The rule for such malignant causes of cord and cauda equina compression is gadolinium enhancement of the soft tissue lesions. When in the ventral epidural space, a relatively slow-growing malignancy may demonstrate the suggestive but not specific draped curtain sign, caused by preservation of the midline central septum (anterior meningovertebral ligament) (FIGURE 10-6). This sign may also be observed in indolent infectious processes such as tuberculosis,[25] whereas more rapidly aggressive epidural disease processes, such as epidural infection (phlegmon, abscess) or hematoma, may lack this sign because of violation of the midline ligament.[26] Uncommonly encountered extradural disease processes include conditions such as extramedullary hematopoiesis, Erdheim-Chester disease, idiopathic hypertrophic pachymeningitis, and calcifying pseudoneoplasm of the neuraxis (FIGURE 10-3).

Intradural-Extramedullary Compartment

A multitude of disease processes can occur in the intradural-extramedullary compartment of the spinal canal.

INTRADURAL-EXTRAMEDULLARY NEOPLASMS. Lesions occurring in the intradural-extramedullary compartment can be diagnosed by their widening of the subarachnoid space ipsilaterally and, when large enough, compression/displacement of the spinal cord and effacement of the subarachnoid space contralaterally (FIGURE 10-8). Fortunately, such intradural-extramedullary lesions are most commonly benign. For enhancing intradural-extramedullary masses, the two most likely possibilities are meningiomas and nerve root sheath tumors (schwannomas and neurofibromas).[27] Distinguishing between these entities can be challenging, but certain clues can suggest the correct diagnosis. As for virtually any enhancing lesion in the spine, metastatic disease is in the differential diagnosis.

MENINGIOMAS. Spinal meningiomas are most common in the thoracic spine and most often lateral to the cord.[27] Characteristic, although not entirely specific,

KEY POINTS

- For enhancing intradural-extramedullary masses, the two most likely possibilities are meningiomas and nerve root sheath tumors (schwannomas and neurofibromas).
- Characteristic, although not entirely specific, imaging findings suggestive of spinal meningioma include dural tail(s) of contrast enhancement and avid and homogeneous enhancement of the lesion, which may be relatively T2 hypointense because of cellularity or calcification.

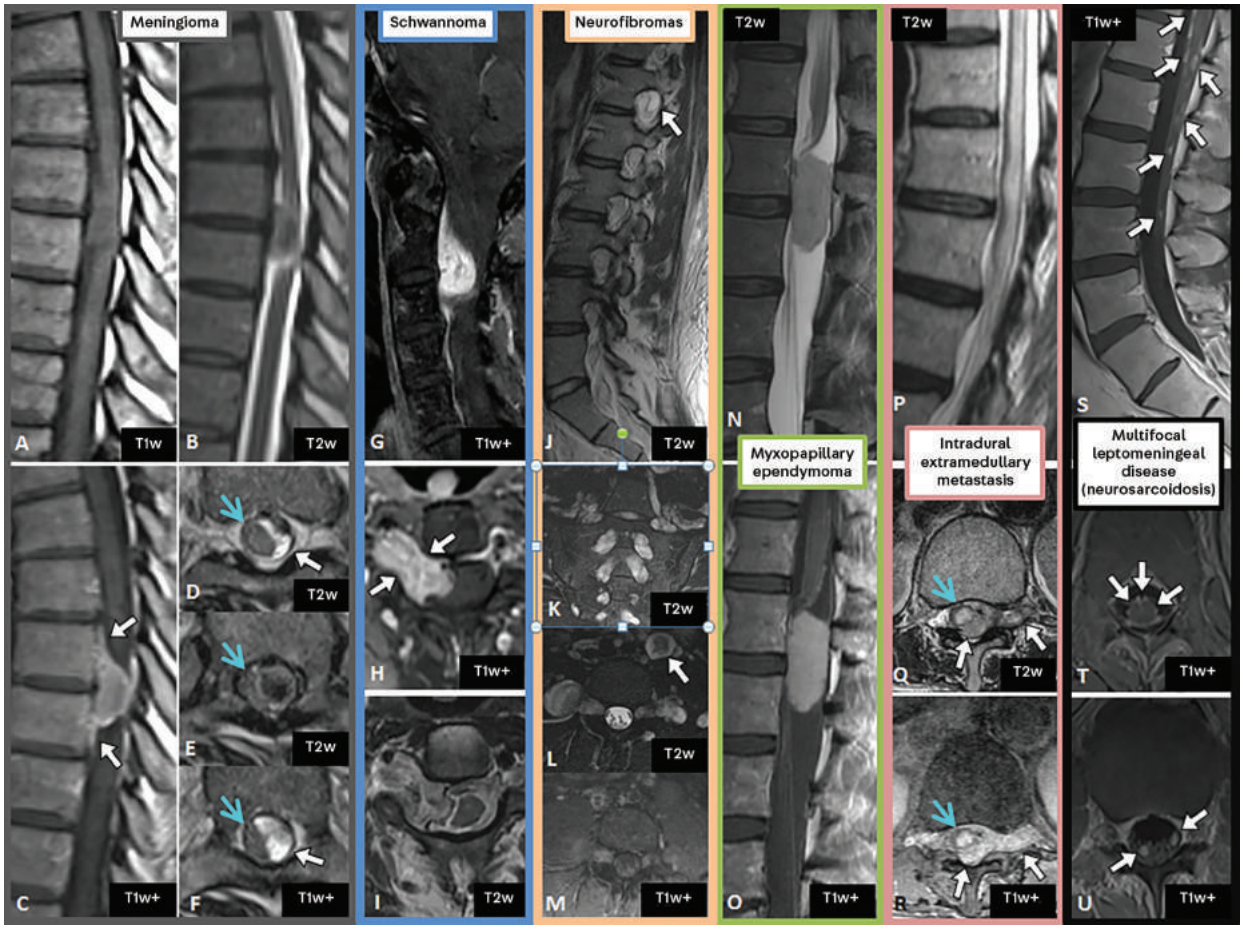

FIGURE 10-8

Intradural-extramedullary disease. Meningiomas (*A* through *F*) may be relatively T2 hypointense (*B*, *E*) because of their high cellularity or calcification. They tend to enhance avidly postcontrast (*C*, *F*) and may have adjacent enhancing dural tails (*C, white arrows*). Axial images demonstrate the characteristic features of intradural-extramedullary masses; the ipsilateral subarachnoid space is expanded immediately above and below the lesion (*D*, *F*, *white arrows*, respectively), with displacement of the spinal cord contralaterally (*D* through *F, blue arrows*). At the level of the lesion, the spinal cord is significantly compressed (*E, blue arrow*), whereas the T2-hypointense lesion fills the adjacent subarachnoid space. Benign nerve sheath tumors (schwannomas [*G* through *I*] and neurofibromas [*J* through *M*]) can be difficult to differentiate. This cervical schwannoma enhances avidly (*G*, *H*), extends through and expands the neural foramen, fills the subarachnoid space, and displaces the spinal cord contralaterally (*I*). Neurofibromas may similarly extend through and expand neural foramina, as is true for many lesions in this patient with neurofibromatosis type 1 (eg, *J, white arrow*). These tumors may characteristically be centrally relatively T2 hypointense and peripherally relatively T2 hyperintense (target sign; *L, white arrow*). Myxopapillary ependymomas (*N*, *O*) classically present as well-defined, avidly enhancing oval masses of the tip of the conus, proximal cauda equina, or filum terminale. Although focal intradural-extramedullary lesions are typically benign, low grade, or slow growing (such as meningiomas, nerve sheath tumors, and myxopapillary ependymomas), intradural-extramedullary metastases (*P* through *R*) can occur in this compartment. The metastasis in this patient causes extensive T2 hyperintensity in the spinal cord (*P*, *Q*; *Q, blue arrow*), with associated focal cord enhancement (*R, blue arrow*). The lesion is heterogeneously signaling and enhancing and occupies the subarachnoid space and neural foramen (*Q*, *R, white arrows*). Multifocal leptomeningeal disease (*S* through *U*) presenting as multifocal smooth or nodular enhancement is not diagnostically specific and can be benign or malignant. Among benign causes, neurosarcoidosis is in the differential diagnosis. This patient with neurosarcoidosis has both smooth pial enhancement along the conus and multifocal nodular enhancement along the cauda equina (*S* through *U, white arrows*).

imaging findings suggestive of spinal meningioma include dural tail(s) of contrast enhancement and avid and homogeneous enhancement of the lesion, which may be relatively T2 hypointense because of cellularity or calcification (FIGURE 10-8). In the authors' clinical experience, spinal meningiomas have a propensity to calcify, although the literature suggests this is uncommon. Multiple lesions are less common than solitary lesions and usually suggest neurofibromatosis type 2 or, much less commonly, meningiomatosis.

NERVE SHEATH TUMORS. Benign nerve sheath tumors (schwannomas and neurofibromas) are well-circumscribed neoplasms that can be difficult to differentiate by imaging. Schwannomas are more prevalent than neurofibromas. When located at least partially in the neural foramen, dumbbell morphology is a characteristic feature (FIGURE 10-8). Schwannomas have a higher propensity to demonstrate cystic change or intratumoral hemorrhage than either neurofibromas or meningiomas. A classic appearance of a neurofibroma is a peripherally T2-hyperintense lesion that is relatively T2 hypointense centrally, the so-called target sign (FIGURE 10-8). Multiple schwannomas can be seen in neurofibromatosis type 2 or, less commonly, schwannomatosis, whereas multiple neurofibromas can occur in neurofibromatosis type 1. When an isolated, incidental, small enhancing nodule of the cauda equina nerve roots is encountered, the most likely consideration is a nerve sheath tumor. Malignant peripheral nerve sheath tumors are rare. Although these tumors often have a heterogeneous appearance, they may mimic the appearance of their benign counterparts, particularly since they too are usually well-circumscribed.[27]

MYXOPAPILLARY EPENDYMOMAS. The most common neoplasm of the region of the tip of the conus, proximal cauda equina, and filum terminale is the myxopapillary ependymoma, a slow-growing variant of ependymoma.[27] This usually intradural-extramedullary neoplasm typically occurs along the filum terminale, can be solitary or multiple, and usually has a characteristic appearance. Myxopapillary ependymomas are usually relatively large, oval or sausage shaped, well circumscribed, T2 hyperintense, and avidly enhancing (FIGURE 10-8). The tumors may contain blood products, causing heterogeneous signal characteristics. Owing to the neoplasm's vascular nature, subarachnoid hemorrhage may be present as a fluid-debris level in the cul-de-sac or superficial siderosis. The less common paraganglioma can mimic the appearance of ependymoma.

MENINGEAL METASTATIC AND INFECTIOUS/INFLAMMATORY DISEASE. The presence of one or more enhancing nodules along the surface of the cord/conus, cauda equina nerve roots, or dura may reflect a metastatic or infectious/inflammatory/toxic process (FIGURE 10-8). Enhancement is the rule for metastatic disease, which is more commonly because of hematogenous dissemination than from drop metastases from a more cephalad, usually intracranial, central nervous system (CNS) primary malignancy. Extensive nodular coating of the pial surface of the cord can occur, the so-called *Zuckerguss* appearance (German for sugarcoating). Enhancing metastatic lesions in other anatomic locations on the MRI and identification of the primary malignancy itself can help make the diagnosis of metastatic disease. Although nodular or nonuniform thickening is typical, diffuse smooth enhancement of the cord surface, cauda equina, or dura

KEY POINTS

- When an isolated, incidental, small enhancing nodule of the cauda equina nerve roots is encountered, the most likely consideration is a nerve sheath tumor.
- Myxopapillary ependymomas are usually relatively large, oval or sausage shaped, well circumscribed, T2 hyperintense, and avidly enhancing.

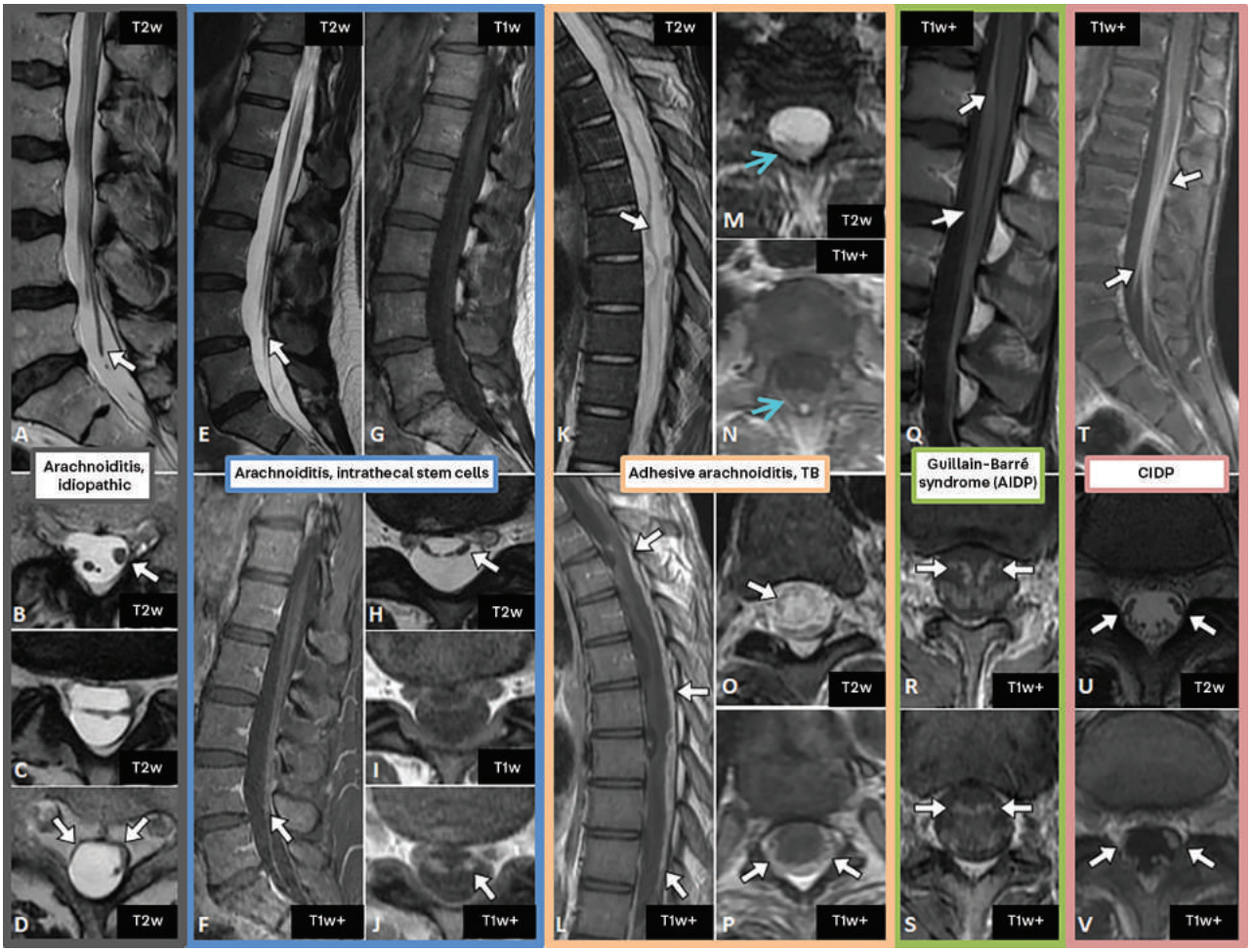

FIGURE 10-9

Arachnoiditis and inflammatory demyelinating polyneuropathies. Arachnoiditis (*A* through *P*, three different patients) can have varying imaging findings and causes. It is often idiopathic (*A* through *D*) or can result from specific irritants within the thecal sac, such as stem cells (*E* through *J*) or infections (*K* through *P*). Thickening or nodularity of cauda equina nerve roots may be evident, best seen on T2-weighted images (*A*, *B*, *E*, *H*, *white arrows*). The nerve roots are commonly nonanatomically distributed (*B* through *D*, *H*) and may be centrally clumped (*C*, *H*) or dispersed peripherally (empty thecal sac sign, *D, white arrows*). Abnormal enhancement is often only mild if present (*F*, *J, white arrows*). Adhesive arachnoiditis (*K* through *P*) such as that caused by infections (including tuberculosis) may cause bizarre appearances related to adhesions and loculations in the thecal sac, altered CSF dynamics, and effects on the spinal cord. The spinal cord may be displaced (*M*, *N, blue arrows*) and may contain T2 hyperintensity or a syrinx (*K*, *O, white arrows*). Thickening and enhancement of the meninges, including the dura, may be observed (*L*, *P, white arrows*). Acute inflammatory demyelinating polyradiculoneuropathy (AIDP) (*Q* through *S*) and chronic inflammatory demyelinating polyradiculoneuropathy (CIDP) (*T* through *V*) are considerations when thickened (*Q*, *U, white arrows*) or enhancing (*R* through *T, V, white arrows*) nerve roots are encountered but the distribution is anatomic. AIDP has a predilection to involve the ventral nerve roots (*Q* through *S, white arrows*).

can also occur. The latter smooth appearance is not as strongly suggestive for metastatic disease, since infectious/inflammatory/toxic causes are generally more likely to cause such a uniform abnormality than to be nodular.[27] For this diverse group of non-neoplastic disorders, unless ancillary imaging findings such as those discussed in the intramedullary sections below are present, a specific diagnosis often requires alternative tests, particularly CSF analysis.

NON-NEOPLASTIC INTRADURAL-EXTRAMEDULLARY DISEASES OF THE ARACHNOID AND DURA. Among intradural-extramedullary disease processes, several non-neoplastic diseases that can affect the arachnoid and dura are important to recognize.

ARACHNOIDITIS. Irritation of the arachnoid resulting in postinflammatory adhesions can be idiopathic or occur for variety of known reasons, including most commonly as an iatrogenic complication or because of trauma/subarachnoid hemorrhage or inflammation/infection, such as intrathecal stem cell therapy (FIGURE 10-9).[28] Arachnoiditis can have varying imaging presentations and most commonly involves the cauda equina nerve roots. The affected nerve roots may lack the normal anatomic distribution (ie, they do not layer dependently in the supine patient and lack their normal organization). Varied appearances of arachnoiditis include nerve roots that are irregularly clumped, clumped into a mass of neural tissue centrally, or dispersed to the margins of the dura (the empty thecal sac sign) (FIGURE 10-9). The nerve roots may or may not be abnormally thickened or enhancing. If diffusely thickened, particularly if the thickening is marked and symmetric but the distribution is anatomic, chronic inflammatory demyelinating polyradiculoneuropathy (CIDP) is a differential consideration (FIGURE 10-9). Acute inflammatory demyelinating polyradiculoneuropathy (AIDP, Guillain-Barré syndrome) can also present with thickened nerve roots; the ventral cauda equina nerve roots are typically asymmetrically affected and often enhance, and the pial surface of the conus may also enhance (FIGURE 10-9).[29] Adhesive arachnoiditis is a severe end-stage manifestation of inflammatory processes such as infections, leading to adhesions and loculations in the thecal sac (FIGURE 10-9). When involving the cervicothoracic spine, the spinal cord can be affected by displacement, myelomalacia, T2 hyperintensity, or syrinx. Arachnoiditis ossificans is a rare, chronic, and severe manifestation of arachnoiditis; the intradural calcifications are often best appreciated on CT.[30]

ARACHNOID/DURAL LESIONS CAUSING EXPANSION OF THE DORSAL ASPECT OF THE THECAL SAC, DORSAL CORD FLATTENING, OR VENTRAL CORD DISPLACEMENT. Abnormalities of arachnoid and dura can result in abrupt distortions of the cord that are difficult to resolve on MRI. The CSF space is typically widened, and the cord displaced without evident mass lesion. Myelography can be useful in more precisely depicting the fine detail and flow dynamics of the extramedullary abnormality.

Arachnoid cysts. Arachnoid cysts can occur in other compartments of the spinal canal but are usually intradural-extramedullary. The most common location for an arachnoid cyst is dorsal to the thoracic cord; although these lesions tend to be well circumscribed, their wall is often imperceptible, especially on MRI (FIGURE 10-10). As a result, and since their signal characteristics are generally isointense to CSF (fluid-type high T2 signal, low T1 signal), they may be difficult

KEY POINTS

- Varied appearances of arachnoiditis include nerve roots that are irregularly clumped, clumped into a mass of neural tissue centrally, or dispersed to the margins of the dura (the empty thecal sac sign).
- The most common location for an arachnoid cyst is dorsal to the thoracic cord; although these lesions tend to be well circumscribed, their wall is often imperceptible, especially on MRI.

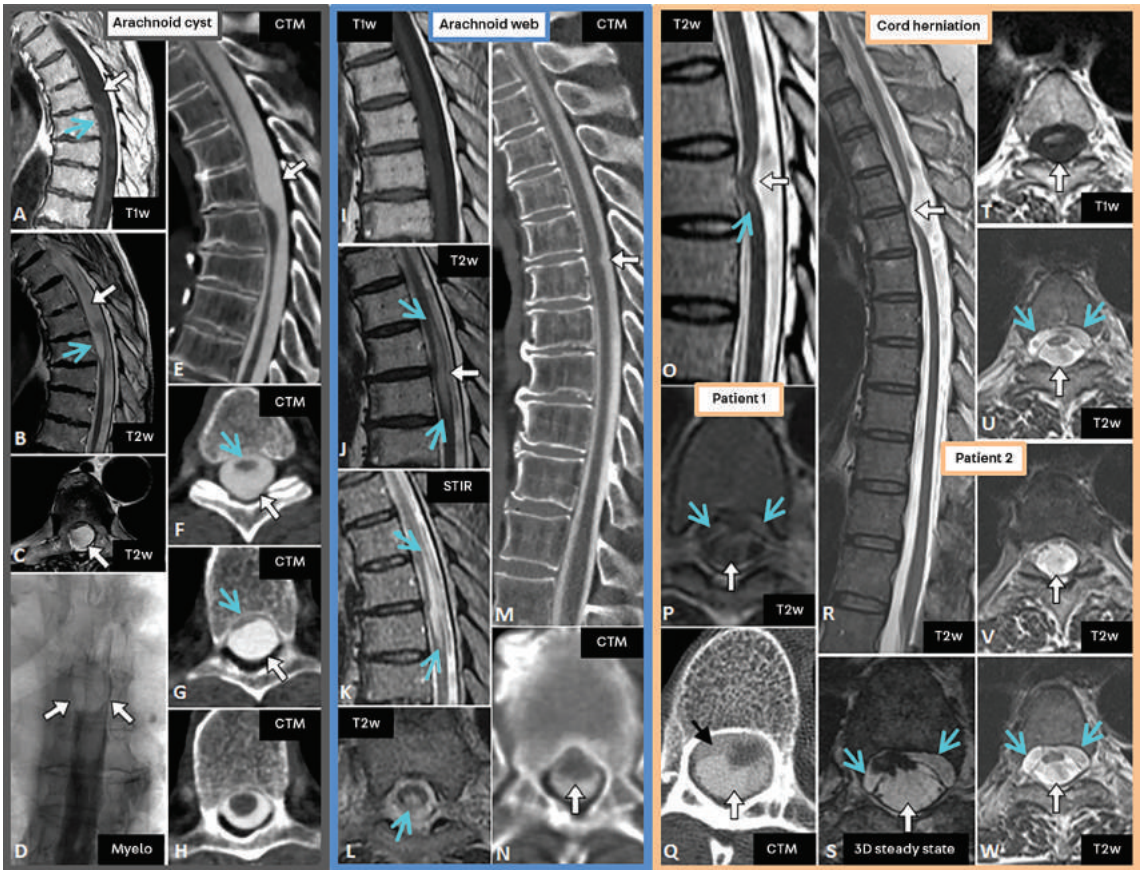

FIGURE 10-10

Dorsal cord flattening: spectrum of disease. Arachnoid cysts (*A* through *H*), arachnoid webs (*I* through *N*), and idiopathic spinal cord herniation (*O* through *Q*, *R* through *W*, two different patients) can all cause flattening of the dorsal aspect of the spinal cord and apparent expansion of the dorsal subarachnoid space. Spinal cord T2 hyperintensity or syrinx formation can be present with any of these entities, such as the syrinx seen in the case of arachnoid cyst (*A*, *B*, *blue arrows*). On MRI, expansion of the dorsal subarachnoid space (*A* through *C*, *white arrows*) is associated with ventral displacement and dorsal flattening of the cord, well seen axially (*C*). On fluoroscopic myelographic visualization before CT myelography, a filling defect is observed (*D*, *white arrows*) consistent with an arachnoid cyst; by the time the patient has been transferred to CT, the arachnoid cyst has filled with contrast (*E* through *G*, *white arrows*). The walls of the cyst are not visualized on either MRI or CT myelography. Spinal cord compression can be observed, just as on MRI (*G*, *blue arrow*). Above this level of maximal mass effect, the spinal cord is ventrally displaced and atrophic (*F*, *blue arrow*), whereas below it the caliber is normal (*H*). Arachnoid webs classically present with a sharply marginated dorsal cord contour irregularity; this is sometimes better seen on CT myelography than MRI (scalpel sign; *M*, *N*, compared to *J*, *white arrows*). As with other causes of myelopathic signal abnormality, spinal cord T2 hyperintensity (*J* through *L*, *blue arrows*) is seen to slightly better advantage on short tau inversion recovery (STIR) than conventional T2-weighted images (*K* compared to *J*, *blue arrows*). The arachnoid web itself is not visualized. Idiopathic spinal cord herniation has similar imaging findings to arachnoid cysts and webs, including dorsal cord contour irregularity and expansion of the dorsal subarachnoid space (*O* through *Q*, *R* through *W*, *white arrows*, two different patients) as well as spinal cord T2 hyperintensity (*O*, *blue arrow*). Extreme ventral cord positioning on sagittal images with loss of subarachnoid space between the cord and posterior aspect of the vertebral bodies/disk can be a clue (*O*, *R*) and is best evaluated on axial images, which can better show the herniation of the spinal cord through the dura (*P* through *Q*; *S*). Prominent ventral extradural fluid is an additional clue (*P*, *blue arrows*; *Q*, *black arrow*; *S*, *U*, *W*, *blue arrows*). Thin-section heavily T2-weighted three-dimensional steady state sequences can be useful to depict the focal ventral transdural cord herniation in high resolution (*S*).

to visualize on MRI. Indeed, in some cases, the mass effect that they may cause on the spinal cord may be the primary clue to their presence. Because of their chronic nature, arachnoid cysts may remodel or expand the spinal canal in benign fashion. Because they also can be dynamic lesions that may fill rapidly or slowly, sophisticated imaging techniques may be required to diagnose arachnoid cysts confidently, including conventional myelography under fluoroscopy with real-time visualization in the early phase of opacification of the spinal canal with contrast (FIGURE 10-10), multipositional CT myelography, and delayed images on either modality. On MRI, thin-section heavily T2-weighted images can also be helpful (TABLE 10-2).

Arachnoid webs. Arachnoid webs are lesions of unknown etiology that may be closely related to arachnoid cysts. Some postulate that these may represent the incomplete/disrupted formation of an arachnoid cyst.[31] Such webs are bands of arachnoid tissue along the dorsal aspect of the spinal cord, most commonly occurring in the upper to midthoracic spine. The band itself is only rarely demonstrated on imaging. Typically, arachnoid webs cause mass effect on and flattening of the dorsal cord, with a characteristic but not pathognomonic morphology termed the scalpel sign that is best seen sagittally on either T2-weighted images or CT myelography (FIGURE 10-10). The initial and largest series to date describing this sign included 14 patients, but nine were not surgically proven.[31] Indeed, it can be difficult or, in some cases, impossible to confidently differentiate arachnoid cysts and webs, despite high-resolution MRI and CT myelography.

Idiopathic spinal cord herniation. The spinal cord may herniate through a defect in the dura into the extradural compartment (FIGURE 10-10).[32] Such herniation typically occurs ventrally in the thoracic spine (usually T4 through T7) and in many, but not all, cases at a disk space level.[33] In some cases, diskal calcification or osteophytes at the disk space level probably erode the dura and result in the cord herniation. Making the diagnosis is important because surgical treatment may allow reversal or at least stabilization of neurologic deficits. On MRI or CT myelography, the characteristic findings of idiopathic spinal cord herniation include ventral displacement of a short segment of cord that is focally distorted/kinked, with the subarachnoid space being lost ventrally and expanded dorsally (FIGURE 10-10). A ventral extradural CSF collection (leak) may be present. An arachnoid cyst may also be coexistent. Differentiating between a dorsal arachnoid cyst that displaces the cord ventrally and ventral cord herniation with or without an arachnoid cyst can be challenging. Just as is the case for diagnosis of arachnoid cysts and webs, thin-section heavily T2-weighted images on MRI can be helpful (FIGURE 10-10). CT myelography is often required, but in subtle/challenging cases, especially when an arachnoid cyst is coexistent, confident and correct diagnosis may be elusive until surgery.

Intramedullary (Intrinsic) Compartment

When spinal cord signal abnormality is intrinsic in nature without a causative lesion external to the spinal cord, arriving at the correct diagnosis is often more challenging. Such disease processes can be broadly divided into neoplastic and non-neoplastic categories. For these diseases, a detailed analysis of the imaging features of the spinal cord lesion itself as well as the noncord structures may help in arriving at the correct diagnosis or limiting the list of differential conditions.

KEY POINTS

- Typically, arachnoid webs cause mass effect on and flattening of the dorsal cord, with a characteristic but not pathognomonic morphology termed the scalpel sign that is best seen sagittally on either T2-weighted images or CT myelography.
- On MRI or CT myelography, the characteristic findings of idiopathic spinal cord herniation include ventral displacement of a short segment of cord that is focally distorted/kinked, with the subarachnoid space being lost ventrally and expanded dorsally.

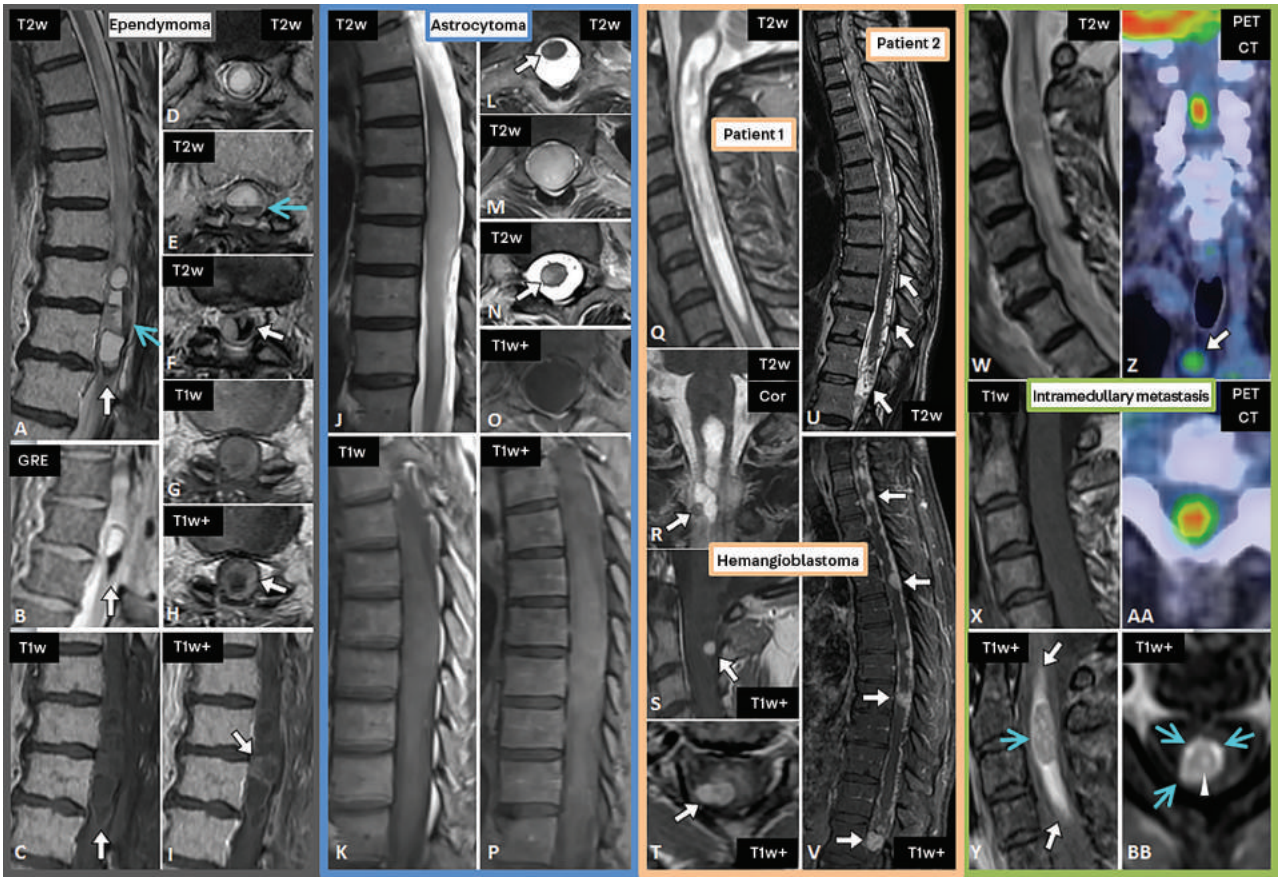

FIGURE 10-11

Intramedullary neoplastic myelopathy. Ependymomas (*A* through *I*) are expansile neoplasms that may demonstrate blood products, including as T1- and T2-hypointense regions at the margin of the tumor (*cap sign*; *A*, *C*, *F, white arrows*); this is related to hemosiderin content, which blooms or becomes more pronounced on gradient recalled echo (GRE) images (*B, white arrow*). Blood products may also layer dependently as blood-fluid levels (*A*, *E, blue arrows*). One clue for ependymoma over astrocytoma is the centrally located nature of the tumor (*D*). Ependymomas tend to enhance (*H*, *I, white arrows*). Astrocytomas (*J* through *P*) tend to be eccentrically located, which may be most evident at the margins of the expansile neoplasm (*L*, *N*, *white arrows*, at slices along the superior and inferior aspects of the tumor, compared to *M* at a slice in the midportion). Enhancement may be absent or minimal (*O*, *P*). Hemangioblastomas (*Q* through *T*, *U* and *V*, two different patients) typically have a markedly different appearance compared to ependymomas and astrocytomas. The lesions are often located on the dorsal cord surface, avidly enhancing, and small (*R* through *T, white arrows*), especially with regard to the extensive spinal cord T2 hyperintensity, syrinx, or cysts they produce (*Q*, *R*). Lesions can be multiple (*V, white arrows*) and may have significant associated vascularity, well seen as hypointense flow voids in the CSF on T2-weighted images (*U, white arrows*). Like hemangioblastomas, intramedullary spinal cord metastases (*W* through *BB*) can produce significant cord T2 hyperintensity for neoplasm size (*W* compared to *Y*). The lesions may demonstrate one or more of three characteristic enhancement features: a rim of more intense enhancement around the enhancing mass (rim sign; *Y*, *BB, blue arrows*); ill-defined flame-shaped enhancement at the superior or inferior, or both, margins of the lesion (flame sign; *Y, white arrows*); and a punctate focus of enhancement in/near the center of the lesion (central dot sign; *BB, arrowhead*). On fludeoxyglucose positron emission tomography (FDG-PET), spinal cord metastases are typically FDG avid (*Z*, *AA*); just as on MRI, other evidence for metastatic disease may be present (*Z*, *white arrow*, a metastatic paratracheal lymph node from a lung carcinoma).

Relevant features include the cross-sectional pattern of involvement (white matter versus gray matter versus both), the longitudinal extent of the lesion (short versus long), expansion (presence or absence), associated findings in the spinal cord (such as hemorrhage, cysts, and other lesions), enhancement (presence and pattern, if present), and findings outside the spinal canal (such as in the osseous vertebral column, paraspinal regions, and extraspinal regions).

Broadly speaking, differentiating neoplastic from non-neoplastic intrinsic cord lesions may not always be possible, but several features can be helpful. Neoplasms tend to expand the spinal cord, to have a mass or masslike appearance, and to enhance.[34] The presence of associated adjacent cord cysts or hemorrhage typically suggests a neoplastic process. Such features are not perfect, however. For example, occasionally neoplasms are ill-defined/infiltrative appearing, and occasionally non-neoplastic diseases are tumorlike. Similarly, a long-segment abnormality with patchy enhancement favors a non-neoplastic process, but neoplasms can also be quite extensive with patchy/ill-defined enhancement, especially astrocytomas.

INTRAMEDULLARY NEOPLASMS. Primary cord neoplasms are more common than metastases. The three most common primary cord neoplasms are ependymoma, astrocytoma, and hemangioblastoma. Ependymoma is the most common primary cord neoplasm in adults, whereas astrocytoma predominates in children. Other primary tumors, such as gangliogliomas and spinal cord lymphomas, are not discussed here.

EPENDYMOMAS. Ependymomas arise from the ependymal lining of the central canal of the spinal cord. Thus, these neoplasms typically have a central location within the spinal cord. They tend to be well-circumscribed expansile lesions (FIGURE 10-11). Enhancement is typically present and often well defined. Internal or adjacent heterogeneity, including related to the presence of cystic change (polar cyst) or hemorrhage (T2-hypointense hemosiderin cap sign) at the margins of the lesion, is more commonly encountered with ependymoma than with astrocytoma (FIGURE 10-11). Spinal cord ependymomas can be seen in patients with neurofibromatosis type 2.

ASTROCYTOMAS. Astrocytomas are the second most common primary cord neoplasm in adults. In contrast to ependymomas, these expansile tumors tend to be eccentrically rather than centrally located (FIGURE 10-11) and are more likely to be poorly defined. If a tumor is holocord, it is more likely to be an astrocytoma than an ependymoma. Although astrocytomas usually enhance, they may not; when they do enhance, it may be fairly mild in amount/intensity or ill-defined (FIGURE 10-11). Hemorrhage is not a common feature. Spinal cord astrocytomas can be seen in patients with neurofibromatosis type 1.

HEMANGIOBLASTOMAS. The third most common primary spinal cord tumor in adults is the hemangioblastoma. These neoplasms are highly vascular and can occur sporadically or in the setting of von Hippel-Lindau disease. They can be solitary or multiple (FIGURE 10-11) and intramedullary or intradural-extramedullary. Because of their vascular nature, avid enhancement is the rule, and prominent vascularity may be evident as flow voids, especially on T2-weighted images within or adjacent to the lesion (FIGURE 10-11).

KEY POINTS

- **Neoplasms tend to expand the spinal cord, to have a mass or masslike appearance, and to enhance. The presence of associated adjacent cord cysts or hemorrhage typically suggests a neoplastic process.**
- **Internal or adjacent heterogeneity, including related to the presence of cystic change (polar cyst) or hemorrhage (T2-hypointense hemosiderin cap sign) at the margins of the lesion, is more commonly encountered with ependymoma than with astrocytoma.**
- **Although astrocytomas usually enhance, they may not; when they do enhance, it may be fairly mild in amount/intensity or ill-defined.**

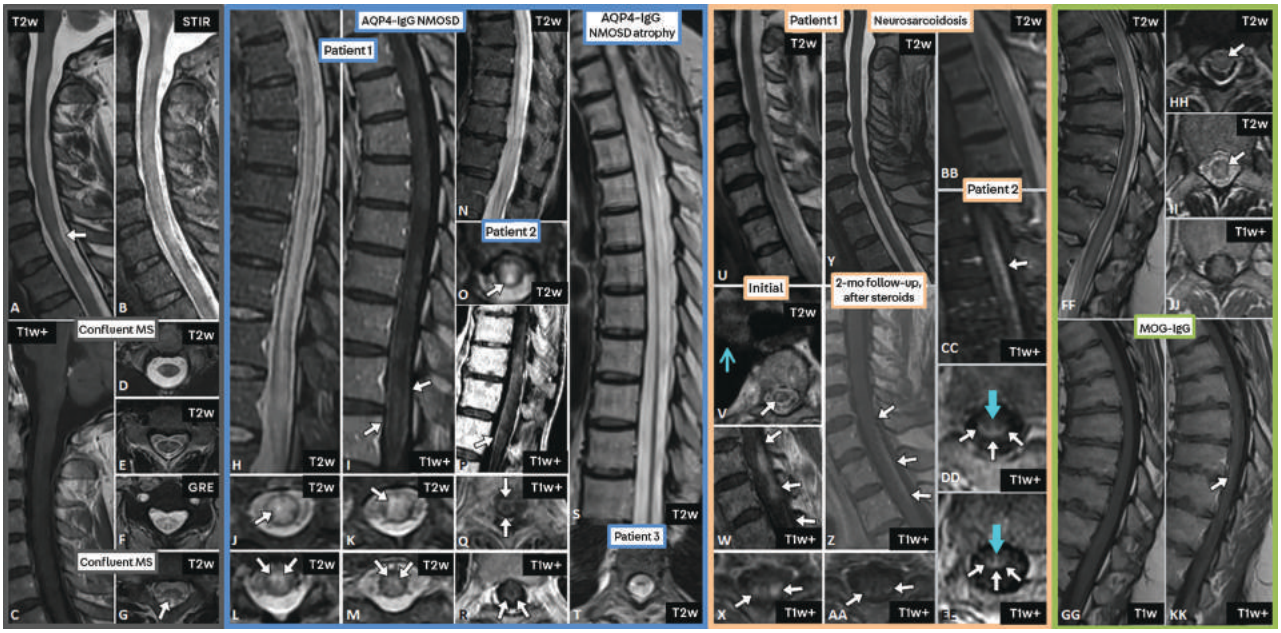

FIGURE 10-12

Longitudinally extensive intramedullary inflammatory/demyelinating myelitis. Long-segment multiple sclerosis is not common, but confluent multiple sclerosis may result from innumerable adjacent T2-hyperintense lesions (*A*, *B*, *D* through *G*), best seen sagittally on short tau inversion recovery (STIR) (*B*) and axially on gradient recalled echo images (GRE) (*F*) compared to traditional T2-weighted images (*A*, *E*). In the chronic phase, the lesions do not enhance (*C*) and atrophy may be evident (*A*, *G, white arrows*). Aquaporin-4-IgG neuromyelitis optica spectrum disorder (NMOSD) (*H* through *M*; *N* through *R*; *S* and *T*, three different patients) characteristically presents as a longitudinally extensive myelitis (*H*, *N*, *S*). Imaging features with relative specificity include small foci on axial images that are at least as T2 hyperintense as CSF (bright spotty lesions; *J* through *M, white arrows*) and ring/partial ring enhancement on sagittal or axial images (*I*, *Q*, *R, white arrows*). Any myelopathy can cause atrophy in the chronic phase, which can be short or long segment (*S*, *T*). Neurosarcoidosis (*U* through *AA*, *BB* through *EE*, two different patients) is also usually long segment (*U*, *BB*). A characteristic enhancement pattern is broad-based involvement of the dorsal subpial/pial aspect of the cord (*W*, *X*, *Z*, *AA*, *CC* through *EE, white arrows*), which may also involve the central canal of the cord (*DD*, *EE*, *blue arrows*) as best seen on axial images; this concomitant dorsal subpial/pial and central canal enhancement of the cord on axial images is termed the trident sign. When the thoracic spine is imaged, cord T2 hyperintensity/enhancement (*V, white arrow*) may not be the only critical observation; mediastinal/hilar adenopathy can be a clue to the diagnosis (*V, blue arrow*). The spinal cord findings typically are responsive to steroids, but even when improving they can persist for months after treatment has been initiated (*Z*, *AA* compared to *W*, *X, white arrows*). Myelin oligodendrocyte glycoprotein (MOG)-IgG myelitis (*FF* through *KK*) similarly tends to be long segment and commonly involves the thoracolumbar region (*FF*), often with central/gray matter selective involvement (*HH*, *II, white arrows*). Enhancement may be absent (*JJ*) or minimal (*KK, white arrow*), a clue to the diagnosis.

Hemangioblastomas have a propensity to be eccentrically located and abut the surface of the spinal cord, with an enhancing pial/subpial nodule especially dorsally. The neoplasms may present as cystic or partially cystic lesions with nodular enhancement (FIGURE 10-11). Even when small, the lesions can produce a significant amount of abnormal intramedullary T2 hyperintensity, indicating edema, syringohydromyelia, or cyst formation (FIGURE 10-11). Evidence of prior hemorrhage in or along the spinal cord may be present.

METASTASIS. Intramedullary spinal cord metastases are most commonly singular (FIGURE 10-11), with multiple lesions occurring in 20% of patients on initial (index) scans at clinical presentation. Several recently described features of intramedullary spinal cord metastases can help make a specific diagnosis. Two highly specific enhancement characteristics of intramedullary spinal cord metastases are reasonably prevalent in these lesions and not commonly seen in primary cord tumors: the rim and flame signs (FIGURE 10-11).[35] The rim sign refers to a more intense partial or complete rim of enhancement surrounding a less intensely enhancing noncystic/necrotic lesion. The flame sign refers to an ill-defined flame-shaped region of enhancement in the spinal cord along the superior or inferior, or both, aspects of the lesion. A third less prevalent sign is the central dot sign, a punctate focus of intense enhancement at/near the center of an enhancing lesion, seen in a small minority of intramedullary spinal cord metastases but not in primary cord tumors, based on a 2020 study (FIGURE 10-11).[36] The presence of extensive spinal cord T2 hyperintensity with respect to a relatively small lesion size can also be a clue to the diagnosis (FIGURE 10-11) and is a poor prognostic factor,[37] although the aforementioned hemangioblastoma may similarly cause this finding. Hemorrhage and cystic change/necrosis are uncommon in intramedullary spinal cord metastases.[38] Evidence of other metastatic disease (eg, in the bones of the spine or paraspinal regions) or of the primary malignancy (eg, a lung carcinoma) is often present on the index MRI.[38] Intramedullary spinal cord metastases are typically avid on fludeoxyglucose positron emission tomography (FDG-PET) examinations (FIGURE 10-11) but may be underreported on this modality.[39]

NON-NEOPLASTIC INTRAMEDULLARY DISEASES. A plethora of non-neoplastic intramedullary diseases can cause myelopathy. Selected causes that are commonly encountered in clinical practice are discussed first below.

MULTIPLE SCLEROSIS. MS is the prototypical CNS demyelinating disease. MRI of the brain and spinal cord are the paraclinical tests of highest utility for the diagnosis of MS, and they can substitute for clinical data in the determination of dissemination in space or dissemination in time in the setting of a typical clinically isolated syndrome.[40] The 2017 revised McDonald diagnostic criteria for MS allow for both symptomatic and asymptomatic MRI cord lesions to be used for determining dissemination in space or dissemination in time. When MS affects the spinal cord, the lesions tend to be small and multiple (FIGURE 10-12). The cervical cord is more commonly involved than the thoracic cord, and silent MS lesions frequently occur.[41] Characteristically, MS lesions are short segment (less than two segments craniocaudally), asymmetrically and eccentrically located (not involving the entire cross-sectional area), and affect white or white plus gray matter. Common cross-sectional locations include the lateral and dorsal aspects of the cord. Although not pathognomonic, these morphologic and locational features can strongly suggest the diagnosis. As is true for lesions in the brain, enhancement is compatible with active demyelination and can be seen in the acute to subacute phases. This can be of varying morphologies, including ill-defined, solid/nodular, ring, or partial ring. Acute lesions can be expansile but usually not markedly so given their often-small size. Long-segment involvement of the cord is not common in adult patients and is sometimes the result of the confluence of multiple small lesions (FIGURE 10-12).[42]

KEY POINTS

- Hemangioblastomas have a propensity to be eccentrically located and abut the surface of the spinal cord, with an enhancing pial/subpial nodule especially dorsally. The neoplasms may present as cystic or partially cystic lesions with nodular enhancement.
- Two highly specific enhancement characteristics of intramedullary spinal cord metastases are reasonably prevalent in these lesions and not commonly seen in primary cord tumors: the rim and flame signs.
- Characteristically, multiple sclerosis lesions are short segment (fewer than two segments craniocaudally), asymmetrically and eccentrically located (not involving the entire cross-sectional area), and affect white or white plus gray matter. Common cross-sectional locations include the lateral and dorsal aspects of the cord.

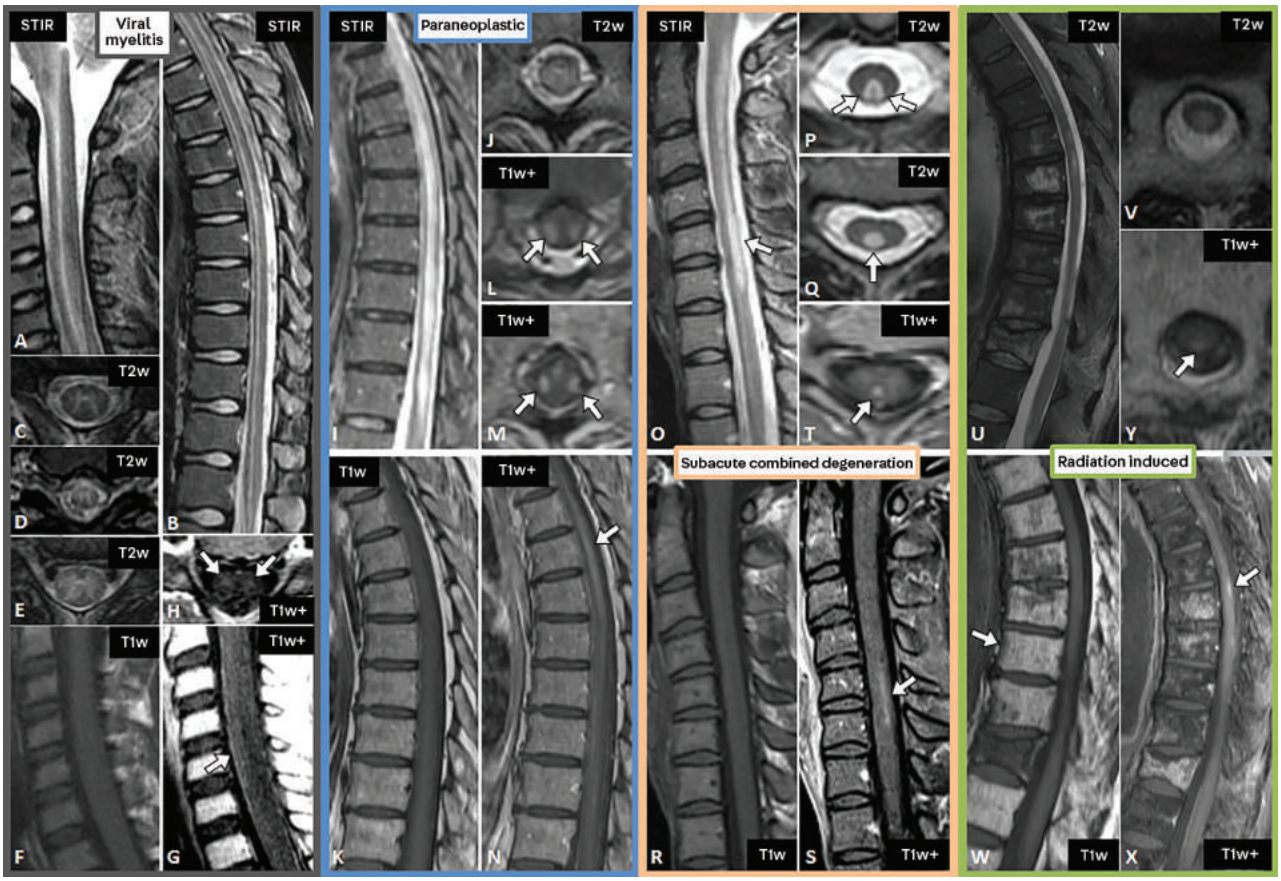

FIGURE 10-13

Intramedullary nontumoral inflammatory myelopathies. Viral myelitis (*A* through *G*) may result in long-segment T2 hyperintensity of the central gray matter (*A* through *E*), which can enhance in the acute phase (*G*, *H, arrows*). Paraneoplastic myelopathy (*I* through *N*) may cause long-segment T2 hyperintensity (*I*, *J*) and enhancement (*L* through *N, arrows*). A clue can be the tract-specific nature of the signal abnormality or of the enhancement, as is evident in this case of lateral column enhancement bilaterally (*L*, *M, arrows*). Subacute combined degeneration (*O* through *T*) characteristically causes T2 hyperintensity of the dorsal columns (*O* through *Q, arrows*). The morphology on axial images may be that of an inverted V or inverted rabbit ears (*P, arrows*). If acute-subacute, the process may be mildly expansile (*O*), and enhancement can occur (*S*, *T, arrows*). Radiation-induced myelopathy (*U* through *X*) can present with nonspecific spinal cord T2 hyperintensity (*U*, *V*), which can be confluent or patchy (*U*), may involve the central cord (*V*), and may enhance (*X*, *Y, arrows*). A key clue is the radiation-induced inherent (precontrast) marrow T1 hyperintensity of the regional spinal column (eg, *W, arrow*). This manifests as very hypointense signal on fat-suppressed T2-weighted (*U*) or T1-weighted postcontrast (*X*) images. The patient shown also has multifocal T1-hypointense enhancing osseous metastases.

LONGITUDINALLY EXTENSIVE MYELITIS (MOST COMMONLY AQP4-IgG–SEROPOSITIVE NMOSD, NEUROSARCOIDOSIS, AND MOG-IgG–ASSOCIATED DISORDER). A commonly encountered scenario is a long-segment myelopathy (three or more segments craniocaudally), with variably expansile T2 hyperintensity and a relative lack of a neoplasmlike appearance. The three primary neuroimaging considerations based on prevalence are AQP4-IgG–seropositive NMOSD, neurosarcoidosis, and MOG-IgG–associated disorder,[43] although other causes exist. For more information, refer to the articles "Myelitis and Other Autoimmune Myelopathies"

by Sebastian Lopez Chiriboga, MD, and Eoin P. Flanagan, MBBCh,[44] and "Infectious Myelopathies" by Michel Toledano, MD,[45] in this issue of *Continuum*.

AQP4-IgG–seropositive NMOSD characteristically causes a long-segment autoimmune myelopathy, with lesions tending to be three or more segments in length and often expansile (FIGURE 10-12). Three characteristic features of AQP4-IgG–seropositive NMOSD that may be present are involvement of the cervicomedullary junction, T1-hypointense components of the lesion, and foci on axial images that are at least as T2 hyperintense as CSF (bright spotty lesions) (FIGURE 10-12).[46-48] The enhancement pattern is often patchy and heterogeneous, and ring or partial ring enhancement (with a prevalence of approximately 30% to 35% among NMOSD cases) can strongly suggest the diagnosis over neurosarcoidosis (FIGURE 10-12).[49,50]

Sarcoidosis is a noncaseating granulomatous disease that can affect any aspect of the neuraxis, including any compartment of the spine. The classic finding of neurosarcoidosis of the cord is a long-segment myelopathy, with characteristic enhancement at the dorsal subpial/pial aspect of the cord (FIGURE 10-12).[51] When such broad contact with the dorsal cord surface is present, the appearance may be plaquelike or sheetlike. When the enhancement also involves the central canal of the spinal cord, a trident sign can be evident axially (FIGURE 10-12).[52] Even during successful treatment, the enhancement may persist (FIGURE 10-12); in a 2016 study, 97% of patients with neurosarcoidosis demonstrated persistent spinal cord enhancement at 2 months after presentation compared to 12% of patients with AQP4-IgG–seropositive NMOSD.[53] The spinal canal may also be positive for enhancing leptomeningeal disease elsewhere, such as thickening (smooth or nodular) of the pial surface or cauda equina nerve roots. Ancillary findings outside of the spinal canal should be sought on the index spinal MRI; these include mediastinal and hilar adenopathy (FIGURE 10-12) and osseous lesions. The latter tend to be lytic or mixed lytic-sclerotic but are not common.[54]

Among other causes of a longitudinally extensive myelopathy, MOG-IgG–associated myelitis can be suggested on MRI. Findings for this inflammatory myelitis are not entirely specific but include more than one lesion, T2 hyperintensity confined to gray matter, preferential involvement of the thoracolumbar region, and lack of or only minimal enhancement (FIGURE 10-12).[43]

OTHER NONTUMORAL INFLAMMATORY MYELOPATHIES. Although not as common as the aforementioned non-neoplastic intramedullary causes of myelopathy, several other intrinsic inflammatory spinal cord diseases are important to recognize.

Viral myelitis/myelopathy. The spinal cord can be affected by a host of infectious diseases, including (but not limited to) viruses. For more information, refer to the article "Infectious Myelopathies" by Michel Toledano, MD,[45] in this issue of *Continuum*. Other infections, including bacterial, fungal, and rare or endemic organisms, such as parasites, are not considered here. Both acute viral infection (myelitis) (FIGURE 10-13) and postviral immunologic reaction (myelopathy) can occur. MRI can be normal.[55] Selective viral involvement of the anterior horn cells can result in acute flaccid paralysis. An example is the 2014 outbreak related to enterovirus D68, with its resultant viral myelitis typically characterized by long-segment T2 hyperintensity of the central gray matter, particularly in the cervical cord.[56] Other viruses with such predilection include polioviruses,

KEY POINTS

- Three characteristic features of aquaporin-4-IgG–seropositive neuromyelitis optica spectrum disorder that may be present are involvement of the cervicomedullary junction, T1-hypointense components of the lesion, and foci on axial images that are at least as T2 hyperintense as CSF (bright spotty lesions).
- The enhancement pattern in aquaporin-4-IgG–seropositive neuromyelitis optica spectrum disorder is often patchy and heterogeneous, and ring or partial ring enhancement can strongly suggest the diagnosis over neurosarcoidosis.
- The classic finding of neurosarcoidosis of the cord is a long-segment myelopathy, with characteristic enhancement at the dorsal subpial/pial aspect of the cord.
- Selective viral involvement of the anterior horn cells can result in acute flaccid paralysis. An example is the 2014 outbreak related to enterovirus D68, which typically resulted in long-segment T2 hyperintensity of the central gray matter, particularly in the cervical cord.

coxsackieviruses, enterovirus 71, West Nile virus, Japanese B encephalitis virus, and tick-borne encephalitis virus.[56] A second primary form of clinical presentation is mixed motor and sensory dysfunction due to involvement of white matter or gray matter, or both. This pattern can be seen with infections such as herpes simplex virus type 2, varicella-zoster virus, cytomegalovirus, Epstein-Barr virus, rabies, and coxsackieviruses. Human immunodeficiency virus (HIV) can present with a vacuolar myelopathy that has a predilection for the lateral and posterior columns, but it can also involve the central aspects of the cord, including gray matter; neither of these presentations typically enhance.[57] Viral myelitis/myelopathy tends to be long segment and can be asymmetric or symmetric on axial images (FIGURE 10-13). The T2 hyperintensity may be expansile in nature, and enhancement of the cord or the adjacent meninges or nerve roots may be present in the acute-early subacute phase (FIGURE 10-13). If present, hemorrhagic necrosis manifests as heterogeneous signal abnormality, potentially including hyperintensity on T1-weighted images.[58] Viral (and other types of CNS infections) can also involve the cauda equina nerve roots, which may be diffusely thickened or enhancing.

Paraneoplastic myelopathy. A rare but likely underreported and underrecognized immune-mediated cause of myelopathy is a paraneoplastic syndrome most commonly associated with lung and breast carcinomas. When present, the spinal cord T2 hyperintensity of paraneoplastic myelopathy is often long segment, symmetric, and tract specific, such as confined to the lateral or dorsal columns (FIGURE 10-13).[59] The gray matter can also be involved. Because of tract specificity, the appearance may be relatively linear on sagittal images. Enhancement after gadolinium administration may be present and may also be tract specific (FIGURE 10-13).[60] An extraspinal primary neoplasm or evidence of metastatic disease can be a clue to the diagnosis. Other autoimmune causes of myelopathy can have an identical appearance to paraneoplastic myelopathy.

TOXIC-METABOLIC-IATROGENIC MYELOPATHY. An important category of intrinsic myelopathy is that which includes toxic, metabolic, and iatrogenic causes.

SUBACUTE COMBINED DEGENERATION. Subacute combined degeneration of the spinal cord due to vitamin B_{12} deficiency has multiple potential causes, including primary vitamin B_{12} deficiency (pernicious anemia), inadequate vitamin B_{12} intake, and nitrous oxide toxicity. The characteristic feature on MRI is selective involvement of the dorsal columns (FIGURE 10-13); the lateral columns may also be involved. MRI is relatively insensitive for subacute combined degeneration but, when positive, demonstrates T2 hyperintensity of the dorsal columns with an inverted V or inverted rabbit ears morphology on axial images, especially in the cervical and upper thoracic cord (FIGURE 10-13).[61] If the lateral columns are also involved, a three-point sign may be present. In the acute-subacute phase, the cord may be mildly enlarged, without or with enhancement (FIGURE 10-13). With prompt treatment, the cord findings typically resolve, although not always. The differential of a posterior/posterolateral column syndrome includes (but is not limited to) copper deficiency,[62] vitamin E deficiency, heroin-induced myelopathy, methotrexate toxicity, and HIV myelopathy.

RADIATION-INDUCED MYELOPATHY. Radiation-induced myelopathy is rare. It is a dose-dependent complication of radiation therapy and can manifest in an acute, early delayed, or late time frame. When present, MRI features include nonspecific confluent spindle-shaped or fusiform spinal cord T2 hyperintensity, with or without expansion. Characteristically, the lateral spinothalamic tracts and dorsal columns are affected, but the involvement can also be patchy and can include the central cord (FIGURE 10-13). Parenchymal enhancement may be present (FIGURE 10-13). In the chronic phase, nonspecific atrophy or cystic myelomalacia may be present. A key ancillary imaging clue for radiation-induced myelopathy is associated vertebral body marrow T1 hyperintensity (fatty marrow replacement) encompassing the radiation port (FIGURE 10-13).[63] Cauda equina involvement with abnormal enhancement of the nerve roots may also occur as a sequela of radiation.

VASCULAR MYELOPATHY. Although a myriad of vascular diseases may affect the spinal cord, the two most commonly encountered clinically and on neuroimaging are spinal cord infarcts and spinal dural arteriovenous fistulas. The clinical presentation and imaging findings are distinct. For more information on vascular disease affecting the spinal cord, refer to the article "Vascular Myelopathies" by Nicholas L. Zalewski, MD,[64] in this issue of *Continuum*.

SPINAL CORD INFARCT. Spinal cord infarcts most commonly affect the thoracic cord and conus, typically in an anterior spinal artery distribution (FIGURE 10-14). MRI may be normal acutely. DWI of the spine is technically challenging compared to of the brain; however, it can be sensitive even very early in the course of the disease. Similar to arterial infarcts in the brain, restricted diffusion (with high signal on DWI and low signal on apparent diffusion coefficient images) can be seen in acute spinal cord infarcts (FIGURE 10-14). On T2-weighted images of an anterior spinal artery infarct, preferential involvement of the gray matter manifests as an H-shaped or butterfly-shaped appearance (FIGURE 10-14), or as an owl-eyes or snake-eyes sign.[65] Central gray matter involvement is highly characteristic but not pathognomonic, as diseases such as acute viral myelitis or Hirayama disease can have a similar appearance. The less common posterior spinal artery cord infarct involves the posterolateral one-third of the cord, dorsal columns, and posterior horns. In the early hyperacute-acute phases of spinal cord infarcts, parenchymal T2 signal hyperintensity is usually nonexpansile, thin, and pencil-like on sagittal images.[65] In the later acute–early subacute phases, cord enlargement may be present. Spinal cord infarcts can demonstrate parenchymal enhancement in the acute-subacute phase, often linearly involving the anterior gray matter (FIGURE 10-14).[66] Hemorrhagic conversion can occur[3] but is not common.[67] Because of the shared blood supply of the spinal cord and vertebral bodies, vertebral body infarcts may be observed, usually 1 to 2 weeks after the initial presentation of spinal cord infarct. These osseous infarcts are characterized by geographic, irregular, often serpiginously marginated regions of vertebral marrow abnormality and enhancement (FIGURE 10-14). Enhancement of the ventral cauda equina roots may be evident in the subacute phase of spinal cord infarct (FIGURE 10-14).[68,69] This finding is of unknown etiology, although potentially caused by wallerian degeneration or direct ischemia. The underlying vascular origin for the infarct can be sought on imaging but is infrequently

KEY POINTS

- When present, the spinal cord T2 hyperintensity of paraneoplastic myelopathy is often long segment, symmetric, and tract specific, such as confined to the lateral or dorsal columns.
- MRI is relatively insensitive for subacute combined degeneration but, when positive, demonstrates T2 hyperintensity of the dorsal columns with an inverted V or inverted rabbit ears morphology on axial images, especially in the cervical and upper thoracic cord.
- A key ancillary imaging clue for radiation-induced myelopathy is associated vertebral body marrow T1 hyperintensity (fatty marrow replacement) encompassing the radiation port.
- Similar to arterial infarcts in the brain, restricted diffusion (with high signal on diffusion-weighted imaging and low signal on apparent diffusion coefficient images) can be seen in acute spinal cord infarcts.
- On T2-weighted images of an anterior spinal artery infarct, preferential involvement of the gray matter manifests as an H-shaped or butterfly-shaped appearance, or as an owl-eyes or snake-eyes sign.
- Because of the shared blood supply of the spinal cord and vertebral bodies, vertebral body infarcts may be observed, usually 1 to 2 weeks after the initial presentation of spinal cord infarct.

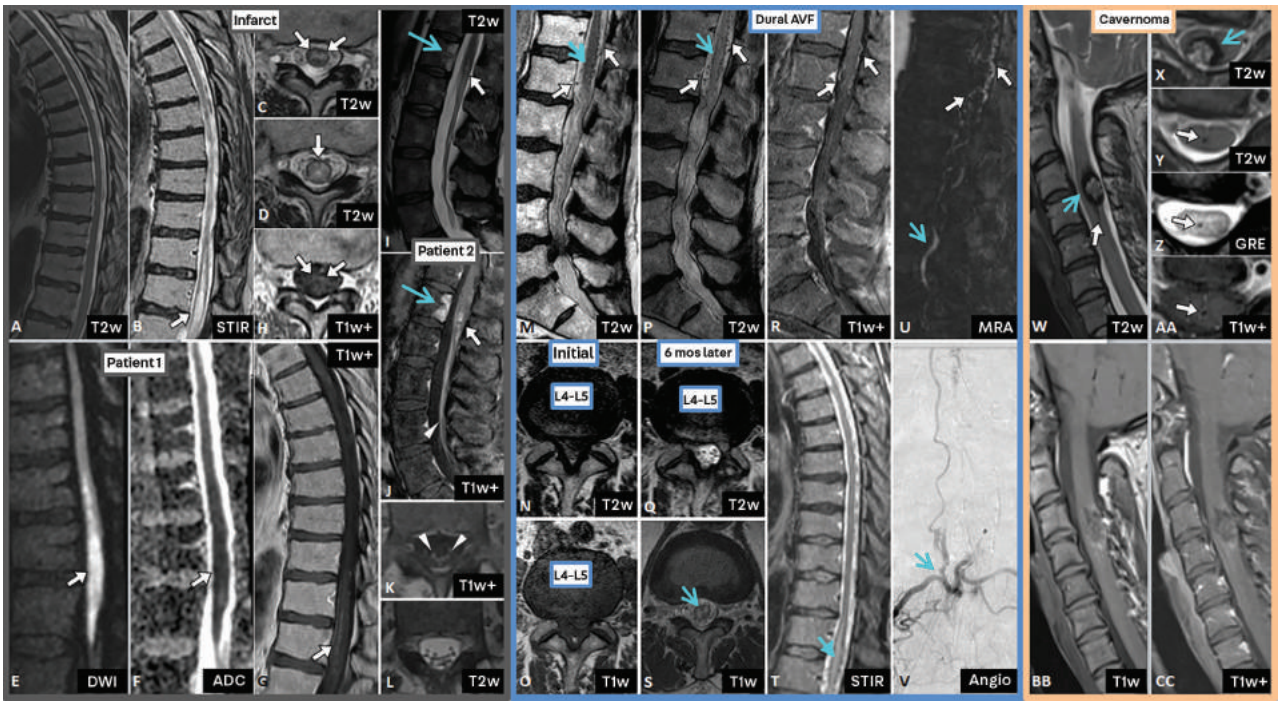

FIGURE 10-14

Vascular myelopathies. Spinal cord infarct (*A* through *G*, *I* through *L*, two different patients) may be MRI negative, especially on conventional T2-weighted images shortly after symptom onset (*A*). In the later acute and early subacute phase, involvement of the thoracic cord/conus by T2 hyperintensity is most common (*B* through *D*, *I*, *white arrows*). An anterior spinal artery infarct commonly affects the gray matter preferentially, with an H-shaped or butterfly-shaped pattern on axial images (*C*, *white arrows*). Markedly hyperintense signal on diffusion-weighted imaging matched by hypointense signal on apparent diffusion coefficient (restricted diffusion, *E*, *F*, *white arrows*) is a key clue for an acute infarct. The infarct may also demonstrate gray matter enhancement in the acute-subacute phase (*G*, *H*, *J*, *white arrows*). Two helpful ancillary findings that may be present, especially in the subacute phase, are vertebral body infarcts (*I*, *J*, *blue arrows*) and cauda equina enhancement (*J*, *K*, *arrowheads*). Spinal dural arteriovenous fistula (*M* through *V*) is an often-missed diagnosis. Key clues are parenchymal T2 hyperintensity, especially of the distal cord/conus sagittally on lumbar spine MRI (*M*, *P*, *blue arrows*) and T2-hypointense flow voids (*M*, *white arrows*) or vascular enhancement (*R*, *white arrows*) along the cord/conus, related to increased pial vascularity. These subtle findings were not detected on this MRI, with the spinal stenosis at L4-L5 (*M* through *O*) being a major distracting feature. Six months after presentation, with the patient now having undergone an L4-L5 laminectomy (*Q*), a lumbar spine and myelopathy protocol thoracic spine MRI were performed. The spinal cord T2 hyperintensity (*P*, *blue arrow*), surface flow voids (*P*, *white arrows*), and vascular enhancement (*R*, *white arrows*) were identified. The parenchymal T2 hyperintensity is well seen on sagittal short tau inversion recovery (STIR) images (*T*, *blue arrow*) and involves the central aspects of the cord on axial images (*S*, *blue arrow*). Magnetic resonance angiography (MRA) shows the abnormal vascularity (*U*, *white arrows*) and suggests an origin for the arteriovenous malformation at L4 (*U*, *blue arrow*), confirmed on conventional angiography upon injection of a common L4 segmental arterial trunk (*V*, *blue arrow*). Cavernous malformations (cavernomas) (*W* through *CC*) usually have heterogeneous signal intensity on both T2-weighted (*W*, *X*) and T1-weighted images (*BB*). This heterogeneity can include inherent T1 hyperintensity due to subacute blood products (*BB*). The lesions may present with partial or complete T2-hypointense rims (*W*, *X*, *blue arrows*). Even more prevalent is relatively linear extension of typically T2-hypointense and often also T1-hypointense blood products in the spinal cord cranially or caudally away from the lesion (*W*, *Y* through *AA*, *white arrows*). Enhancement of cavernous malformations is usually either lacking (*CC*) or minimal, when allowing for inherent T1 hyperintensity.

evident on MRI, MRA, CT angiography, or conventional angiography; after full imaging and clinical workup, the cause of a spinal cord infarct frequently remains occult.

SPINAL DURAL ARTERIOVENOUS FISTULA. Spinal dural arteriovenous fistulas are the most common type of spinal cord vascular malformation. They typically represent a single arterial-to-venous shunt at a thoracic or lumbar radicular artery in the dural nerve root sleeve and can occur anywhere from the vertebral to the internal iliac arteries. This abnormal shunt causes venous hypertension of the spinal cord. Early detection is critical to maximize the chance of a good outcome; however, despite characteristic imaging features, spinal dural arteriovenous fistulas are frequently missed or misdiagnosed.[70] The classic finding of a spinal dural arteriovenous fistula is increased posterior pial serpentine vascularity, typically best seen on T2-weighted sagittal images as prominent flow voids within the dilated veins along the dorsal cord surface (FIGURE 10-14). These flow voids represent a dilated coronal venous plexus and demonstrate enhancement with gadolinium because of slowed flow. They are present in approximately 85% of cases. In strongly suspected but subtle cases, heavily T2-weighted thin-section volumetric sequences may help visualize the flow voids and fistula.[71] Differential considerations for such flow voids include other rare vascular malformations such as arteriovenous malformations and vascular neoplasms such as hemangioblastomas, myxopapillary ependymomas, and paragangliomas. The venous hypertension of the spinal cord parenchyma typically results in edema and expansile cord and conus T2 hyperintensity often sparing the peripheralmost aspect of the cord (FIGURE 10-14), with or without amorphous cord enhancement. The conus is involved in the majority of cases (95%). If the conus is spared, the location of the fistula is likely thoracic.[72] The upper cervical cord may be involved from a posterior fossa arteriovenous fistula. In a 2018 series, enhancement was observed in 86% of cases of spinal dural arteriovenous fistulas, with 43% of these demonstrating a so-called missing piece morphology, which is defined as at least one focal geographic nonenhancing area within a long (more than two vertebral segments) segment of intense holocord (whole cross-sectional area of spinal cord) gadolinium enhancement.[73] MRA with gadolinium-bolus technique can localize or suggest the likely level of the shunting lesion and guide conventional catheter angiography (FIGURE 10-14), thus decreasing the time, radiation dose, and volume of contrast material required to identify the nidus.[74] Catheter angiography is the gold standard imaging technique for diagnosis, allowing localization of the shunt and of the anterior spinal artery. After treatment with embolization or surgery, imaging findings can persist, even if therapy has been successful. Progression of findings, particularly worsening of parenchymal T2 hyperintensity, suggests incomplete treatment or recurrence.[75]

CAVERNOUS MALFORMATION. Cavernous malformations of the cord are tumors related to repetitive hemorrhage and present as mass lesions (FIGURE 10-14). These low-flow vascular lesions are often relatively small at presentation; larger size (>1 cm) is a predictor of subsequent hemorrhage.[76] They can be multiple or synchronously present in the brain, especially in familial cases. The presence of hemorrhage within or adjacent to the lesion is a clue to the diagnosis. Blood products have complex signal characteristics on MRI, which are age dependent. As in the brain, spinal cord cavernous malformations classically may have a

KEY POINTS

- Enhancement of the ventral cauda equina roots may be evident in the subacute phase of spinal cord infarct.
- The classic finding of a spinal dural arteriovenous fistula is increased posterior pial serpentine vascularity, typically best seen on T2-weighted sagittal images as prominent flow voids within the dilated veins along the dorsal cord surface.

KEY POINT

● Adjacent hemorrhage in the spinal cord extending craniocaudally away from a cavernous malformation is relatively prevalent; a 2020 retrospective series demonstrated that this finding is more common than some classic features of these lesions, such as popcorn morphology and T2-hypointense rim.

popcorn-type morphology, with well-circumscribed but lobulated margins and a reticulated core of heterogeneous T1 and T2 signal abnormality. If subacute hemorrhage is present, T1 hyperintensity is expected (FIGURE 10-14). Classically, a T2-hypointense rim representing hemosiderin may surround the lesion (FIGURE 10-14). Sequences sensitive to hemosiderin, such as GRE, will demonstrate pronounced hypointensity (blooming) of the lesion. Spinal cord edema may accompany a cavernous malformation if it has recently bled. Adjacent hemorrhage in the spinal cord extending craniocaudally away from a cavernous malformation is relatively prevalent; a 2020 retrospective series demonstrated that this finding is more common than some of the aforementioned classic features of these lesions, such as popcorn morphology and T2-hypointense rim (FIGURE 10-14).[77] Lesional enhancement is typically either not present or only minimal in degree. The differential diagnosis for a hemorrhagic cord lesion also includes a neoplasm (especially hemangioblastoma or ependymoma) and posttraumatic contusion/hematoma.

CONCLUSION

A rational imaging approach to myelopathy should be employed. MRI is typically first line, and a protocol tailored to the indication is advised. Abnormal T2 hyperintensity of the spinal cord has a broad differential diagnosis. Imaging features should be sought that can help arrive at specific diagnoses or a narrowed list of differential considerations. The process of narrowing the differential diagnosis starts with placing the lesion into one of three compartments: extradural, intradural-extramedullary, and intramedullary. Imaging features of the lesion itself and of the adjacent spinal column, paraspinal soft tissues, and visualized nonspinal regions must be evaluated. Both precontrast and postcontrast MRI can hold clues to the diagnosis. Specific contrast enhancement patterns can be helpful in correctly identifying individual disease processes. CT myelography can help evaluate lesions of the arachnoid and dura, particularly the spectrum of disease that includes arachnoid cyst, arachnoid web, and idiopathic cord herniation. For some conditions that have a dynamic positional component, flexion MRI or upright MRI/CT myelography can be helpful.

REFERENCES

1 Zalewski NL, Flanagan EP, Keegan BM. Evaluation of idiopathic transverse myelitis revealing specific myelopathy diagnoses. Neurology 2018; 90(2):e96-e102. doi:10.1212/WNL.0000000000004796

2 Lee MJ, Aronberg R, Manganaro MS, et al. Diagnostic approach to intrinsic abnormality of spinal cord signal intensity. Radiographics 2019; 39(6):1824-1839. doi:10.1148/rg.2019190021

3 Flanagan EP, Hunt CH, Lowe V, et al. [(18)F]-fluorodeoxyglucose-positron emission tomography in patients with active myelopathy. Mayo Clin Proc 2013;88(11):1204-1212. doi:10.1016/j.mayocp.2013.07.019

4 Vargas MI, Gariani J, Sztajzel R, et al. Spinal cord ischemia: practical imaging tips, pearls, and pitfalls. AJNR Am J Neuroradiol 2015;36(5): 825-830. doi:10.3174/ajnr.A4118

5 Hardy TA. Spinal cord anatomy and localization. Continuum (Minneap Minn) 2021;27(1, Spinal Cord Disorders):12-29.

6 Diehn FE, Maus TP, Morris JM, et al. Uncommon manifestations of intervertebral disk pathologic conditions. Radiographics 2016;36(3):801-823. doi:10.1148/rg.2016150223

7 Zarrabian MM, Diehn FE, Kotsenas AL, et al. Dorsal lumbar disc migrations with lateral and ventral epidural extension on axial MRI: a case series and review of the literature. AJNR Am J Neuroradiol 2016;37(11):2171-2177. doi:10.3174/ajnr.A4875

8 Choi JY, Lee WS, Sung KH. Intradural lumbar disc herniation–is it predictable preoperatively? A report of two cases. Spine J 2007;7(1):111-117. doi:10.1016/j.spinee.2006.02.025

9 Maus T. Imaging the back pain patient. Phys Med Rehabil Clin N Am 2010;21(4):725-766. doi:10.1016/j.pmr.2010.07.004

10 Pierce JL, Donahue JH, Nacey NC, et al. Spinal hematomas: what a radiologist needs to know. Radiographics 2018;38(5):1516-1535. doi:10.1148/rg.2018180099

11 Diehn FE. Imaging of spine infection. Radiol Clin North Am 2012;50(4):777-798. doi:10.1016/j.rcl.2012.04.001

12 Maus TP. Imaging of spinal stenosis: neurogenic intermittent claudication and cervical spondylotic myelopathy. Radiol Clin North Am 2012;50(4):651-679. doi:10.1016/j.rcl.2012.04.007

13 Flanagan EP, Marsh RW, Weinshenker BG. Teaching neuroimages: "pancake-like" gadolinium enhancement suggests compressive myelopathy due to spondylosis. Neurology 2013;80(21):e229. doi:10.1212/WNL.0b013e318293e346

14 Flanagan EP, Krecke KN, Marsh RW, et al. Specific pattern of gadolinium enhancement in spondylotic myelopathy. Ann Neurol 2014;76(1):54-565. doi:10.1002/ana.24184

15 Boet R, Chan YL, King A, et al. Contrast enhancement of the spinal cord in a patient with cervical spondylotic myelopathy. J Clin Neurosci 2004;11(5):512-514. doi:10.1016/j.jocn.2004.02.005

16 Conway BL, Clarke MJ, Kaufmann TJ, Flanagan EP. Utility of extension views in spondylotic myelopathy mimicking transverse myelitis. Mult Scler Relat Disord 2017;11:62-64. doi:10.1016/j.msard.2016.12.004

17 Stino AM, LoRusso SJ. Myelopathies due to structural cervical and thoracic disease. Continuum (Minneap Minn) 2018;24(2, Spinal Cord Disorders):567-583. doi:10.1212/CON.0000000000000594

18 Barz T, Melloh M, Staub LP, et al. Nerve root sedimentation sign: evaluation of a new radiological sign in lumbar spinal stenosis. Spine (Phila Pa 1976) 2010;35(8):892-897. doi:10.1097/BRS.0b013e3181c7cf4b

19 Wang G, Peng Z, Li J, et al. Diagnostic performance of the nerve root sedimentation sign in lumbar spinal stenosis: a systematic review and meta-analysis. Neuroradiology 2019;61(10):1111-1121. doi:10.1007/s00234-019-02248-3

20 Lehman VT, Luetmer PH, Sorenson EJ, et al. Cervical spine MR imaging findings of patients with Hirayama disease in North America: a multisite study. AJNR Am J Neuroradiol 2013;34(2):451-456. doi:10.3174/ajnr.A3277

21 Boruah DK, Prakash A, Gogoi BB, et al. The importance of flexion MRI in Hirayama disease with special reference to laminodural space measurements. AJNR Am J Neuroradiol 2018;39(5):974-980. doi:10.3174/ajnr.A5577

22 Hirayama K, Tokumaru Y. Cervical dural sac and spinal cord in juvenile muscular atrophy of distal upper extremity. Neurology 2000;54(10):1922-1926. doi:10.1212/wnl.54.10.1922

23 Huang YL, Chen CJ. Hirayama disease. Neuroimaging Clin N Am 2011;21(4):939-50, ix-x. doi:10.1016/j.nic.2011.07.009

24 Chen CJ, Hsu HL, Tseng YC, et al. Hirayama flexion myelopathy: neutral-position MR imaging findings–importance of loss of attachment. Radiology 2004;231(1):39-44. doi:10.1148/radiol.2311030004

25 Strauss SB, Gordon SR, Burns J, et al. Differentiation between tuberculous and pyogenic spondylodiscitis: the role of the anterior meningovertebral ligament in patients with anterior epidural abscess. AJNR Am J Neuroradiol 2020;41(2):364-368. doi:10.3174/ajnr.A6370

26 Kim DH, Rosenblum JK, Panghaal VS, et al. Differentiating neoplastic from nonneoplastic processes in the anterior extradural space. Radiology 2011;260(3):825-830. doi:10.1148/radiol.11102287

27 Koeller KK, Shih RY. Intradural extramedullary spinal neoplasms: radiologic-pathologic correlation. Radiographics 2019;39(2):468-490. doi:10.1148/rg.2019180200

28 Madhavan AA, Summerfield D, Hunt CH, et al. Polyclonal lymphocytic infiltrate with arachnoiditis resulting from intrathecal stem cell transplantation. Neuroradiol J 2020;33(2):174-178. doi:10.1177/1971400920902451

29 Mohajeri Moghaddam S, Bhatt AA. Location, length, and enhancement: systematic approach to differentiating intramedullary spinal cord lesions. Insights Imaging 2018;9(4):511-526. doi:10.1007/s13244-018-0608-3

30 Anderson TL, Morris JM, Wald JT, Kotsenas AL. Imaging appearance of advanced chronic adhesive arachnoiditis: a retrospective review. AJR Am J Roentgenol 2017;209(3):648-655. doi:10.2214/AJR.16.16704

31 Reardon MA, Raghavan P, Carpenter-Bailey K, et al. Dorsal thoracic arachnoid web and the "scalpel sign": a distinct clinical-radiologic entity. AJNR Am J Neuroradiol 2013;34(5):1104-1110. doi:10.3174/ajnr.A3432

32 Haber MD, Nguyen DD, Li S. Differentiation of idiopathic spinal cord herniation from CSF-isointense intraspinal extramedullary lesions displacing the cord. Radiographics 2014;34(2):313-329. doi:10.1148/rg.342125136

33 Brus-Ramer M, Dillon WP. Idiopathic thoracic spinal cord herniation: retrospective analysis supporting a mechanism of diskogenic dural injury and subsequent tamponade. AJNR Am J Neuroradiol 2012;33(1):52-56. doi:10.3174/ajnr.A2730

34 Koeller KK, Rosenblum RS, Morrison AL. Neoplasms of the spinal cord and filum terminale: radiologic-pathologic correlation. Radiographics 2000;20(6):1721-1749. doi:10.1148/radiographics.20.6.g00nv151721

35 Rykken JB, Diehn FE, Hunt CH, et al. Rim and flame signs: postgadolinium MRI findings specific for non-CNS intramedullary spinal cord metastases. AJNR Am J Neuroradiol 2013;34(4):908-915. doi:10.3174/ajnr.A3292

36 Madhavan AA, Diehn FE, Rykken JB, et al. The central dot sign: a specific post-gadolinium enhancement feature of intramedullary spinal cord metastases. Clin Neuroradiol. Published online May 7, 2020. doi:10.1007/s00062-020-00909-y

37 Diehn FE, Rykken JB, Wald JT, et al. Intramedullary spinal cord metastases: prognostic value of MRI and clinical features from a 13-year institutional case series. AJNR Am J Neuroradiol 2015;36(3):587-593. doi:10.3174/ajnr.A4160

38 Rykken JB, Diehn FE, Hunt CH, et al. Intramedullary spinal cord metastases: MRI and relevant clinical features from a 13-year institutional case series. AJNR Am J Neuroradiol 2013;34(10):2043-2049. doi:10.3174/ajnr.A3526

39 Mostardi PM, Diehn FE, Rykken JB, et al. Intramedullary spinal cord metastases: visibility on PET and correlation with MRI features. AJNR Am J Neuroradiol 2014;35(1):196-201. doi:10.3174/ajnr.A3618

40 Thompson AJ, Banwell BL, Barkhof F, et al. Diagnosis of multiple sclerosis: 2017 revisions of the McDonald criteria. Lancet Neurol 2018;17(2):162-173. doi:10.1016/S1474-4422(17)30470-2

41 Traboulsee A, Simon JH, Stone L, et al. Revised Recommendations of the Consortium of MS Centers Task Force for a Standardized MRI Protocol and Clinical Guidelines for the Diagnosis and Follow-Up of Multiple Sclerosis. AJNR Am J Neuroradiol 2016;37(3):394-401. doi:10.3174/ajnr.A4539

42 Asnafi S, Morris PP, Sechi E, et al. The frequency of longitudinally extensive transverse myelitis in MS: a population-based study. Mult Scler Relat Disord 2020;37:101487. doi:10.1016/j.msard.2019.101487

43 Dubey D, Pittock SJ, Krecke KN, et al. Clinical, radiologic, and prognostic features of myelitis associated with myelin oligodendrocyte glycoprotein autoantibody. JAMA Neurol 2019;76(3):301-309. doi:10.1001/jamaneurol.2018.4053

44 Lopez Chiriboga S, Flanagan EP. Myelitis and other autoimmune myelopathies. Continuum (Minneap Minn) 2021;27(1, Spinal Cord Disorders):62-92.

45 Toledano M. Infectious myelopathies. Continuum (Minneap Minn) 2021;27(1, Spinal Cord Disorders):93-120.

46 Yonezu T, Ito S, Mori M, et al. "Bright spotty lesions" on spinal magnetic resonance imaging differentiate neuromyelitis optica from multiple sclerosis. Mult Scler 2014;20(3):331-337. doi:10.1177/1352458513495581

47 Chee CG, Park KS, Lee JW, et al. MRI features of aquaporin-4 antibody-positive longitudinally extensive transverse myelitis: insights into the diagnosis of neuromyelitis optica spectrum disorders. AJNR Am J Neuroradiol 2018;39(4):782-787. doi:10.3174/ajnr.A5551

48 Pekcevik Y, Mitchell CH, Mealy MA, et al. Differentiating neuromyelitis optica from other causes of longitudinally extensive transverse myelitis on spinal magnetic resonance imaging. Mult Scler 2016;22(3):302-311. doi:10.1177/1352458515591069

49 Zalewski NL, Morris PP, Weinshenker BG, et al. Ring-enhancing spinal cord lesions in neuromyelitis optica spectrum disorders. J Neurol Neurosurg Psychiatry 2017;88(3):218-225. doi:10.1136/jnnp-2016-314738

50 Yokote H, Nose Y, Ishibashi S, et al. Spinal cord ring enhancement in patients with neuromyelitis optica. Acta Neurol Scand 2015;132(1):37-41. doi:10.1111/ane.12354

51 Nesbit GM, Miller GM, Baker HL Jr, et al. Spinal cord sarcoidosis: a new finding at MR imaging with Gd-DTPA enhancement. Radiology 1989;173(3):839-843. doi:10.1148/radiology.173.3.2813795

52 Zalewski NL, Krecke KN, Weinshenker BG, et al. Central canal enhancement and the trident sign in spinal cord sarcoidosis. Neurology 2016;87(7):743-744. doi:10.1212/WNL.0000000000002992

53 Flanagan EP, Kaufmann TJ, Krecke KN, et al. Discriminating long myelitis of neuromyelitis optica from sarcoidosis. Ann Neurol 2016;79(3):437-447. doi:10.1002/ana.24582

54 Soni N, Bathla G, Pillenahalli Maheshwarappa R. Imaging findings in spinal sarcoidosis: a report of 18 cases and review of the current literature. Neuroradiol J 2019;32(1):17-28. doi:10.1177/1971400918806634

55 Grill MF. Infectious myelopathies. Continuum (Minneap Minn) 2018;24(2, Spinal Cord Disorders):441-473. doi:10.1212/CON.0000000000000597

56 Maloney JA, Mirsky DM, Messacar K, et al. MRI findings in children with acute flaccid paralysis and cranial nerve dysfunction occurring during the 2014 enterovirus D68 outbreak. AJNR Am J Neuroradiol 2015;36(2):245-250. doi:10.3174/ajnr.A4188

57 Rovira A, Auger C. Spinal cord in multiple sclerosis: magnetic resonance imaging features and differential diagnosis. Semin Ultrasound CT MR 2016;37(5):396-410. doi:10.1053/j.sult.2016.05.005

58 Yokota H, Yamada K. Viral infection of the spinal cord and roots. Neuroimaging Clin N Am 2015;25(2):247-258. doi:10.1016/j.nic.2015.01.005

59 Zalewski NL, Flanagan EP. Autoimmune and paraneoplastic myelopathies. Semin Neurol 2018; 38(3):278-289. doi:10.1055/s-0038-1660856

60 Madhavan AA, Carr CM, Morris PP, et al. Imaging review of paraneoplastic neurologic syndromes. AJNR Am J Neuroradiol 2020;41(12):2176-2187. doi: 10.3174/ajnr.A6815

61 Schwendimann RN. Metabolic and toxic myelopathies. Continuum (Minneap Minn) 2018; 24(2, Spinal Cord Disorders):427-440. doi:10.1212/ CON.0000000000000596

62 Kumar N, Ahlskog JE, Klein CJ, Port JD. Imaging features of copper deficiency myelopathy: a study of 25 cases. Neuroradiology 2006;48(2): 78-83. doi:10.1007/s00234-005-0016-5

63 Khan M, Ambady P, Kimbrough D, et al. Radiation-induced myelitis: initial and follow-up MRI and clinical features in patients at a single tertiary care institution during 20 years. AJNR Am J Neuroradiol 2018;39(8):1576-1581. doi:10.3174/ajnr. A5671

64 Zalewski NL. Vascular myelopathies. Continuum (Minneap Minn) 2021;27(1, Spinal Cord Disorders): 30-61.

65 Kranz PG, Amrhein TJ. Imaging approach to myelopathy: acute, subacute, and chronic. Radiol Clin North Am 2019;57(2):257-279. doi:10.1016/j.rcl.2018.09.006

66 Zalewski NL, Rabinstein AA, Krecke KN, et al. Characteristics of spontaneous spinal cord infarction and proposed diagnostic criteria. JAMA Neurol 2019;76(1):56-63. doi:10.1001/jamaneurol.2018.2734

67 Laur O, Nandu H, Titelbaum DS, et al. Nontraumatic spinal cord compression: MRI primer for emergency department radiologists. Radiographics 2019;39(6):1862-1880. doi:10.1148/rg.2019190024

68 Diehn FE, Hunt CH, Lehman VT, et al. Vertebral body infarct and ventral cauda equina enhancement: two confirmatory findings of acute spinal cord infarct. J Neuroimaging 2015; 25(1):133-135. doi:10.1111/jon.12058

69 Zalewski NL, Rabinstein AA, Krecke KN, et al. Spinal cord infarction: clinical and imaging insights from the periprocedural setting. J Neurol Sci 2018;388:162-167. doi:10.1016/j.jns.2018.03.029

70 Brinjikji W, Nasr DM, Morris JM, et al. Clinical outcomes of patients with delayed diagnosis of spinal dural arteriovenous fistulas. AJNR Am J Neuroradiol 2016;37(2):380-386. doi:10.3174/ajnr.A4504

71 Morris JM, Kaufmann TJ, Campeau NG, et al. Volumetric myelographic magnetic resonance imaging to localize difficult-to-find spinal dural arteriovenous fistulas. J Neurosurg Spine 2011; 14(3):398-404. doi:10.3171/2010.11.SPINE10328

72 Muralidharan R, Saladino A, Lanzino G, et al. The clinical and radiological presentation of spinal dural arteriovenous fistula. Spine (Phila Pa 1976) 2011;36(25):E1641-E1647. doi:10.1097/ BRS.0b013e31821352dd

73 Zalewski NL, Rabinstein AA, Brinjikji W, et al. Unique gadolinium enhancement pattern in spinal dural arteriovenous fistulas. JAMA Neurol 2018;75(12):1542-1545. doi:10.1001/ jamaneurol.2018.2605

74 Luetmer PH, Lane JI, Gilbertson JR, et al. Preangiographic evaluation of spinal dural arteriovenous fistulas with elliptic centric contrast-enhanced MR angiography and effect on radiation dose and volume of iodinated contrast material. AJNR Am J Neuroradiol 2005;26(4):711-718.

75 Muralidharan R, Mandrekar J, Lanzino G, et al. Prognostic value of clinical and radiological signs in the postoperative outcome of spinal dural arteriovenous fistula. Spine (Phila Pa 1976) 2013; 38(14):1188-1193. doi:10.1097/ BRS.0b013e31828b2e10

76 Goyal A, Rinaldo L, Alkhataybeh R, et al. Clinical presentation, natural history and outcomes of intramedullary spinal cord cavernous malformations. J Neurol Neurosurg Psychiatry 2019;90(6):695-703. doi:10.1136/jnnp-2018-319553

77 Panda A, Diehn FE, Kim DK, et al. Spinal cord cavernous malformations: MRI commonly shows adjacent intramedullary hemorrhage. J Neuroimaging 2020;30(5):690-696. doi:10.1111/jon.12738